© 2021. Published by The Company of Biologists Ltd | Development (2021) 148, dev199026. doi:10.1242/dev.199026

RESEARCH ARTICLE

The SRCAP chromatin remodeling complex promotes oxidative metabolism during prenatal heart development

Mingjie Xu[1], Jie Yao[1], Yingchao Shi[1], Huijuan Yi[1], Wukui Zhao[1], Xinhua Lin[2,*] and Zhongzhou Yang[1,3,4,*]

ABSTRACT

Mammalian heart development relies on cardiomyocyte mitochondrial maturation and metabolism. Embryonic cardiomyocytes make a metabolic shift from anaerobic glycolysis to oxidative metabolism by mid-gestation. VHL-HIF signaling favors anaerobic glycolysis but this process subsides by E14.5. Meanwhile, oxidative metabolism becomes activated but its regulation is largely elusive. Here, we first pinpointed a crucial temporal window for mitochondrial maturation and metabolic shift, and uncovered the pivotal role of the SRCAP chromatin remodeling complex in these processes in mouse. Disruption of this complex massively suppressed the transcription of key genes required for the tricarboxylic acid cycle, fatty acid β-oxidation and ubiquinone biosynthesis, and destroyed respirasome stability. Furthermore, we found that the SRCAP complex functioned through H2A.Z deposition to activate transcription of metabolic genes. These findings have unveiled the important physiological functions of the SRCAP complex in regulating mitochondrial maturation and promoting oxidative metabolism during heart development, and shed new light on the transcriptional regulation of ubiquinone biosynthesis.

KEY WORDS: SRCAP chromatin remodeling complex, Znhit1, H2A.Z, Mitochondria, Metabolism, Heart development, Mouse

INTRODUCTION

In mammals, the heart is the first organ to develop in order to establish a functional circulatory system that is vital for organismal growth during embryogenesis (Cui et al., 2018; Waardenberg et al., 2014). Heart development involves complex morphological changes that are tightly and accurately regulated (Bruneau and Srivastava, 2014; Kathiriya et al., 2015). It is increasingly appreciated that mitochondrial function and metabolism play a crucial role in the maturation of cardiomyocytes and heart development (Cheong et al., 2020; Hom et al., 2011; Larsson et al., 1998). However, compared with postnatal cardiomyocytes, the understanding of mitochondrial metabolism and regulation in prenatal cardiomyocytes is largely lacking, and is derived from very limited studies and literature. Our current knowledge is that VHL-HIF signaling favors anaerobic glycolysis from embryonic day (E) 9.5 to E12.5, and subsequently the protein level of HIF1α is profoundly decreased and its promotion of anaerobic glycolysis subsides towards E14.5 (Guimaraes-Camboa et al., 2015; Maroli and Braun, 2020; Menendez-Montes et al., 2016). Meanwhile, mitochondrial maturation and oxidative metabolism including fatty acid β-oxidation and the tricarboxylic acid (TCA) cycle, are boosted in cardiomyocytes. Thus, embryonic cardiomyocytes make a metabolic shift from exclusive anaerobic glycolysis to oxidative metabolism by E14.5. Accordingly, there must exist novel regulators and mechanisms to advance oxidative metabolism in embryonic cardiomyocytes; however, these have not yet been fully discovered.

Coenzyme Q10 (CoQ10 or ubiquinone) is crucial for electron transport chain (ETC) activity and ATP production by shuttling electrons from complexes I and II to complex III (Wang and Hekimi, 2016). The biosynthesis of CoQ10 requires at least 13 genes, and mutations in these genes in human causes primary CoQ10 deficiency and respiratory chain disorders that affect multiple systems – common diseases include encephalopathy and cardiomyopathy (Doimo et al., 2014). So far, little is known about the transcriptional regulation of CoQ10 biosynthesis.

ATP-dependent chromatin remodeling complexes (remodeler) regulate gene expression using energy from ATP hydrolysis to modulate nucleosome dynamics (the packing state of chromatin) (Clapier and Cairns, 2009). Through moving, ejecting or restructuring the composition of nucleosomes, these remodelers participate in the regulation of many biological processes including metabolic pathways (Beckwith et al., 2018; Meng et al., 2013; Morrison, 2020). The SRCAP complex is one of the ATP-dependent chromatin remodeling complexes and controls the replacement of H2A with the histone variant H2A.Z in the nucleosomes to regulate gene expression (Watanabe et al., 2013; Wong et al., 2007). The core components of the SRCAP complex contain SRCAP, Znhit1, YL-1 (also known as Vps72) and H2A.Z (Hota and Bruneau, 2016; Sardiu et al., 2015). Compared with the other chromatin-remodeling complexes such as the SWI/SNF and CHD complexes, understanding of the biological functions of the SRCAP complex in mammalian development is elusive (Cuadrado et al., 2010; Ye et al., 2017; Zhao et al., 2019).

In the present study, we aimed to investigate the regulators and underlying mechanisms of cardiomyocyte oxidative metabolism during embryonic heart development, which led to the identification of the SRCAP remodeler as a pivotal regulator of oxidative metabolism. Disruption of the SRCAP remodeler substantially suppressed the transcription of key genes required for the TCA cycle, fatty acid β-oxidation and CoQ10 biosynthesis, and destroyed the respirasome stability. We found that SRCAP functions through H2A.Z incorporation to activate the expression of those genes involved in metabolic pathways. These findings unveiled the important physiological functions of the SRCAP remodeler in regulating mitochondrial maturation and oxidative metabolism during heart development, and shed new light on the transcriptional regulation of CoQ10 biosynthesis.

[1]State Key Laboratory of Pharmaceutical Biotechnology, Department of Cardiology, Nanjing Drum Tower Hospital, The Affiliated Hospital of Medical School of Nanjing University, Nanjing 210093, China. [2]State Key Laboratory of Genetic Engineering, School of Life Sciences, Zhongshan Hospital, Fudan University, Shanghai, 200438, China. [3]MOE Key Laboratory of Model Animal for Disease Study, Model Animal Research Center, Medical School of Nanjing University, Nanjing, 210093, China. [4]Jiangsu Key Laboratory of Molecular Medicine, Medical School of Nanjing University, Nanjing 210093, China.

*Authors for correspondence (xlin@fudan.edu.cn; zhongzhouyang@nju.edu.cn)

Z.Y., 0000-0002-3272-5255

Handling Editor: Benoit Bruneau
Received 26 November 2020; Accepted 12 March 2021

Development (2021) 148, dev199026. doi:10.1242/dev.199026

RESULTS

A crucial temporal window for mitochondrial maturation and metabolism

To comprehensively and systematically understand the temporal status of mitochondria and metabolism in the embryonic heart, we performed RNA-seq transcriptome profiling and analysis of the mitochondrial ultra-structure and components of respiratory chain complexes of the cardiac ventricles at seven time points during heart development: E10.5, E11.5, E12.5, E13.5, E14.5, E16.5 and E18.5.

The RNA-seq transcriptome profiling study yielded three clusters of genes with distinct expression patterns. Cluster 1 genes were expressed at low levels at E10.5 but thereafter, their expression level kept increasing until E14.5 when the highest amount of expression was observed (Fig. 1A,B). However, the expression of these genes declined dramatically at E16.5 (Fig. 1A,B). Cluster 2 represented

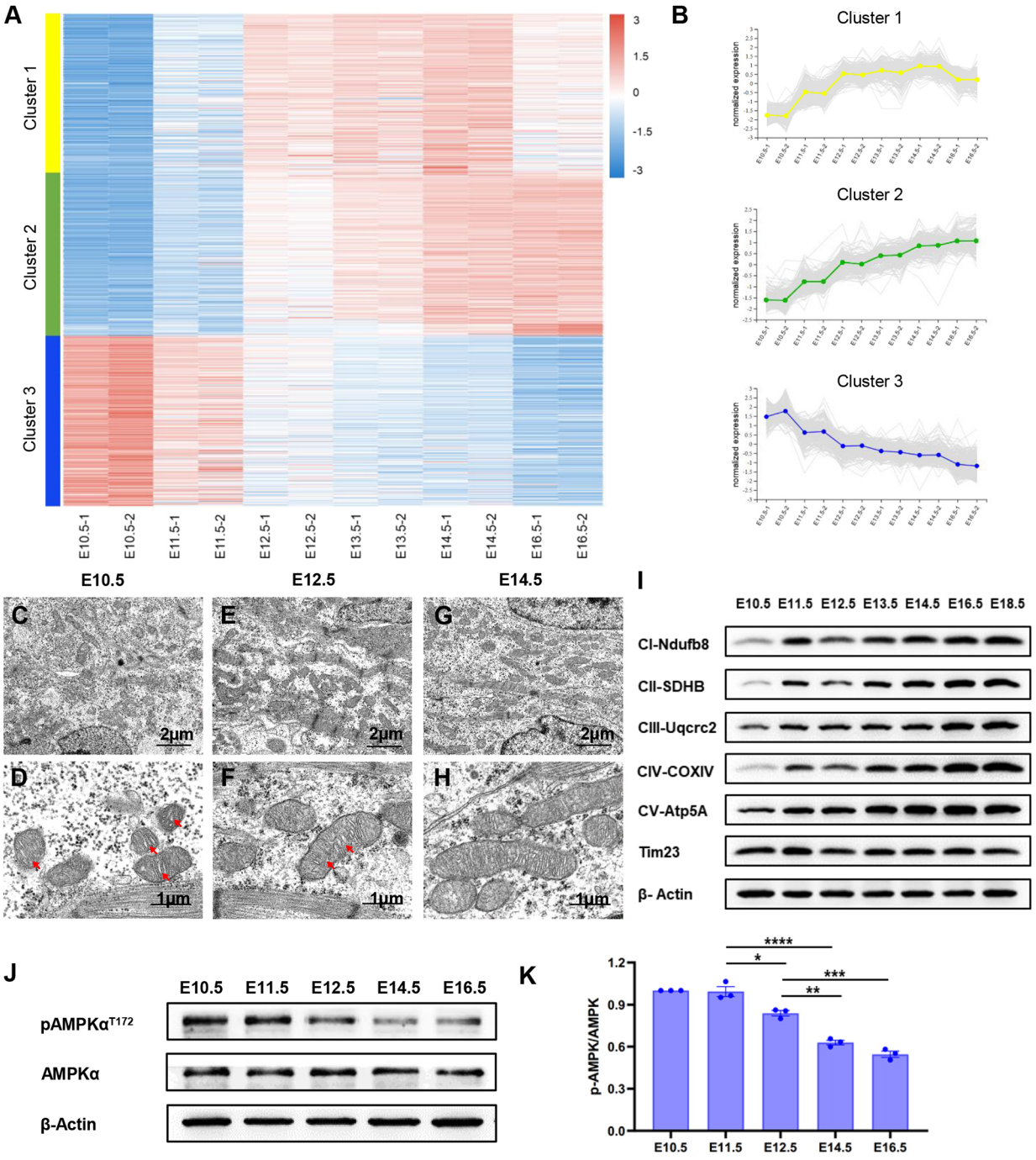

Fig. 1. A crucial temporal window for mitochondrial maturation and metabolism from E11.5 to E14.5. (A,B) RNA-seq transcriptome profiling of ventricular tissues. Heatmap (A) and three clusters of genes categorized using distinct temporal expression patterns (B). (C-H) Transmission electron microscope images of the mitochondria in cardiomyocytes of the left ventricles. D, F and H show higher magnification of panels C, E and G, respectively. The red arrows indicate the bleb/tubular cristae. (I,J) Western blot analysis showing examination of the components of the respiratory super-complexes and Tim23 in the heart tissues (I) and examination of phosphorylated AMPKα^{T172} level in the heart tissues (J). (K) Quantification of J. β-Actin served as loading control. Three independent experiments were repeated, which produced similar results for I-K. Data are mean±s.e.m. *P<0.05, **P<0.01, ***P<0.001, ****P<0.0001 (two-tailed unpaired Student's t-test).

Development (2021) 148, dev199026. doi:10.1242/dev.199026

those genes with early (E10.5-E11.5) expression at similar low levels to cluster 1, but that continued to increase consequently until E16.5 (Fig. 1A,B). Cluster 3 contained genes displaying high level of expression at E10.5, but their expression dropped steadily towards E16.5 (Fig. 1A,B). Representative genes of these three clusters and their biological pathways are summarized in Table 1. It should be noted that many genes in cluster 2 were involved in aerobic metabolism, with expression levels showing a sharp increase from E11.5 to E12.5.

Transmission electronic microscopic (TEM) analysis was conducted to examine the ultrastructure of cardiomyocyte mitochondria during E10.5-E14.5 (Hom et al., 2011). Mitochondria in E10.5 cardiomyocytes manifested immature round morphology enclosing sparse bleb/tubular cristae and a few cristae connected to the periphery (Fig. 1C,D). By E12.5, the cardiomyocyte mitochondria were relatively mature, with many well organized cristae within the rod-like organelle (Fig. 1E,F). Mitochondria in E14.5 cardiomyocytes were elongated (Fig. 1G,H). Abundant stacked laminar cristae appeared in the mitochondria, resembling the mature status in postnatal cardiomyocytes (Fig. 1G,H).

Western blotting analysis was performed to study the dynamic changes of mitochondrial respiratory chain complexes in the myocardium from E10.5 to E18.5. The core subunits of the complexes of I-V (CI-CV) showed profoundly increased protein levels from E10.5 to E11.5, and the amount of these proteins continued to augment until E18.5. The mitochondrial inner membrane protein of Tim23 (Timm23) showed a constant level during the same developmental stages (Fig. 1I).

Furthermore, a specific analysis was carried out to uncover the mitochondrial genes in the RNA-seq transcriptome profiling through comparison with the MitoCarta 2.0 (a database of 1158 nuclear and mtDNA genes whose protein products show eminent support of mitochondrial localization from the Broad Institute of MIT). The result demonstrated that 4.46% of the assayed mRNAs in the RNA-seq transcriptome profiling were mitochondrial and they were predominantly included in clusters 2 and 3. In addition, these mitochondrial genes were categorized into three clusters. Cluster A included genes responsible for assembly of mitochondrial inner membrane and complexes, and associated with tRNA metabolism. The expression level of this cluster declined steadily, suggesting that the process of mitochondrial maturation was approaching completion. Clusters B and C contained a large amount of oxidative metabolic genes, the expression patterns of which indicated that, in the mid-term of gestation, some of them were first activated to regulate metabolic shift and the others were subsequently induced to maintain oxidative metabolism (Fig. S1A,B).

Finally, we examined the protein level of the active AMPKα, a sensor of cellular energy and nutrient status (Hardie, 2014). The result indicated a high activation level of AMPKα at E10.5-E11.5 (Fig. 1J,K). However, from E12.5 its activation level dropped dramatically towards E14.5, indicating a considerable transition from cellular energy deficiency at E11.5 to energy adequacy by E14.5 (Fig. 1J,K).

Collectively, these data have established the panoramic temporal picture of myocardial transcriptome, mitochondrial morphogenesis, respiratory complex and metabolic features spanning from early heart development to the end of embryogenesis. Meanwhile, a crucial time window from E10.5 to E14.5 was pinpointed during which mitochondria became relatively mature and a large amount of the core components of respiratory chain complexes are accumulated in the cardiomyocytes. These results suggest that by E14.5, mitochondrial aerobic metabolism was active and sufficient energy could be generated in the myocardium for cardiac development and function.

Disruption of the SRCAP remodeler impairs heart development

In mammals, the INO80 complex family contains three remodelers: INO80, SRCAP and TRRAP/Tip60 (Kat5) (Clapier and Cairns, 2009). The INO80 remodeler regulates metabolism and it functions to exchange H2A.Z in H2A.Z/H2B dimers with H2A, which can be reversed by the SRCAP chromatin-remodeling complex (Morrison, 2020). Znhit1, one of the core subunits of the SRCAP complex, has been proved to play a crucial role in maintaining the function of the SRCAP complex (Cuadrado et al., 2010; Dong et al., 2014; Ye et al., 2017; Zhao et al., 2019). Here, we first investigated the temporal expression patterns of Znhit1 and the other two core components of the SRCAP remodeler, YL-1 and H2A.Z, in the heart and the results demonstrated significantly increased levels at E11.5 and E12.5, and was consistent with the metabolic shift window defined by us (Fig. S2A,B). Therefore, it is possible that the SRCAP remodeler may modulate the embryonic metabolic switch.

We generated *Znhit1* mutant murine embryonic fibroblasts (MEFs) and detected prominently reduced levels of YL-1 and H2A.Z (Fig. 2A,B). Furthermore, knockdown of *Znhit1* by siRNA in rat H9C2 cells and human HeLa cells also resulted in significantly decreased levels of YL-1 and H2A.Z (Fig. 2C-F). These results demonstrated the important role of Znhit1 in maintaining SRCAP remodeler integrity.

We then deleted *Znhit1* in the cardiomyocytes of the embryonic heart using *Tnnt2-Cre* to investigate the function of SRCAP remodeler in cardiac metabolism and development. Znhit1 was found localized in the nuclei of cardiomyocytes (Fig. S3A). Removal of *Znhit1* in cardiomyocytes (Fig. S3B-D) also impeded the SRCAP

Table 1. Biological pathways and representative genes

	Biological pathways	Representative genes
Cluster 1	Heart valve morphogenesis	*Notch2*, *Tbx20*, *Sox9*, *Dchs1*
	Tube morphogenesis	*Wnt9a*, *Wnt9b*, *Pkd1*, *Pkd2*, *Prrx1*, *Sema5a*
	Cardiac septum morphogenesis	*Sox4*, *Prox1*, *Fzd1*, *Robo1*, *Robo2*
Cluster 2	Regulation of metal ion transport	*Fxyd1*, *Cav1*, *Sln*, *Cacna1g*, *Kcne1*, *Kcnj2*
	Regulation of heart contraction	*Tnnt2*, *Casq2*, *S100a1*, *Tnni3k*, *Adrb1*
	Fatty acid metabolic process	*Ppara*, *Lpl*, *Cpt1b*, *Acot1*, *Acot2*, *Cd36*, *Fabp3*, *Fabp4*, *Fabp7*
	Citrate cycle (tricarboxylic acid cycle)	*Idh2*, *Idh3b*, *Idh3g*, *Mdh1*, *Mdh2*, *Aco2*, *Pdha1*
	Aerobic respiration	*Mb*, *Cox6c*, *Cox8b*, *Uqcrc1*, *Ndufb4c*, *Ndufa4l2*, *Cygb*
Cluster 3	Animal organ morphogenesis	*Wnt4*, *Hand1*, *Tbx2*, *Jag1*, *Bmp2*, *Actn3*, *Cited2*, *Etv2*
	Regulation of cell migration	*Eif5*, *Epor*, *Acta2*, *Itga2b*, *Nog*, *Rnd2*, *Podxl*
	Cell differentiation	*Car2*, *Klf1*, *Bmp5*, *Irx6*, *Wnt2*, *Sema3c*
	Cell fate commitment	*Gata1*, *Gata5*, *Foxc2*, *Wnt11*, *Fgf8*, *Fgf10*

Development (2021) 148, dev199026. doi:10.1242/dev.199026

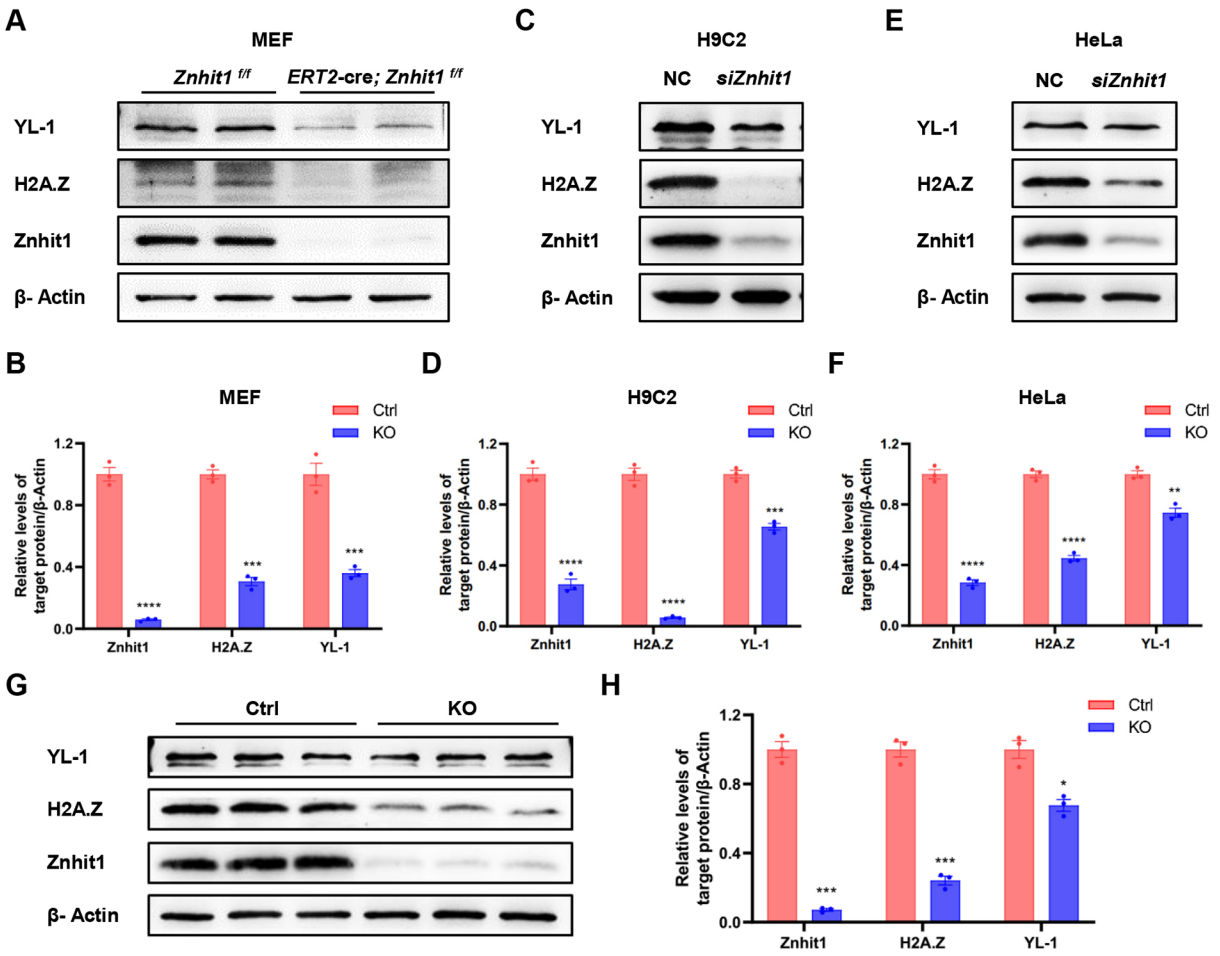

Fig. 2. Removal of *Znhit1* impaired integrity of the SRCAP complex. (A-F) Knockdown of *Znhit1* in different cells: MEF cells, western blot (A) and quantification (B); H9C2 cells, western blot (C) and quantification (D). HeLa cells, western blot (E) and quantification (F). (G,H) Deletion of *Znhit1* in cardiomyocytes (*Tnnt2-Cre* mediated knockout), showing western blot analysis (G) and quantification of G (H). Experiments were repeated independently three times, which produced similar results. Data are mean±s.e.m. **P*<0.05, ***P*<0.01, ****P*<0.001, *****P*<0.0001 (two-tailed unpaired Student's *t*-test).

complex, as shown by reduced protein level of YL-1 and H2A.Z in the heart (Fig. 2G,H). Deletion of *Znhit1* did not affect early heart development by E12.5 (Fig. 3A). However, morphological and histological examination revealed obvious impairment of heart development at E13.5 when the left ventricle was dilated (Fig. 3B-D). At E15.5, the *Znhit1*-deficient heart showed thinned left ventricular myocardium (Fig. 3B-D). By E18.5, the mutant heart displayed features of heart failure (Fig. 3B). All of the *Znhit1*-deficient mice survived to E16.5, but started to die from E17.5. Half of the mice were lost before birth and the rest of them could be born but survived for less than half a day. Expression levels of the key transcription factors for cardiac specification (*Gata4*, *Hand2*, *Tbx5* and *Nkx2-5*) and cardiac contraction regulatory gene (*Tnnt2*) were normal in the mutant heart at E12.5 (Fig. 3E), suggesting that cardiac specification and cardiomyocytes differentiation was not disrupted. In addition, the endocardial-myocardial interface was also unchanged at E12.5 (Fig. 3F). Cell proliferation analysis indicated decreased cardiomyocyte proliferation after E12.5 (Fig. S4A-C). Furthermore, we deleted *Znhit1* using *Mef2c-AHF-Cre* to investigate its role in regulating the development of the second heart field (SHF) progenitors. All of the *Mef2c-AHF-Cre; Znhit1*$^{f/f}$ mice were born with severely malformed right ventricles (Fig. S5A,B). The majority of the mice were lost shortly after birth and only around one-third of them survived beyond 1 week (Fig. S5A). We found that the development of the SHF progenitors was not affected in the early stage, but impaired right ventricles and pulmonary artery stenosis were observed from E13.5 (Fig. S5C). The development of endocardium and endocardial-myocardial interface was fine in *Znhit1*$^{f/f}$*; Mef2c-AHF-Cre* mice at E12.5 and even at E18.5 (Fig. S5D,E). Proliferative capacity of the cardiomyocytes in the right ventricle was not decreased until after E12.5 (Fig. S5F). Furthermore, normal expression levels of the cardiac-specific transcription factors and structural genes indicated unaltered cardiomyocyte differentiation (Fig. S5G). Collectively, these results demonstrate a pivotal role of the SRCAP complex during the mid-to-late period of heart development.

The SRCAP complex maintains the integrity of mitochondrial morphology and respiratory complexes

We performed TEM analysis of the ultra-structure of myocardial mitochondria and the results indicated that deletion of *Znhit1* caused mitochondrial swelling and severe damage to the cristae (Fig. 4A,B). Western blotting analysis showed that, although the protein levels of Ndufb8, SDHB, Uqcrc2, COXII (mt-Co2) and ATP5A increased steadily in control mice from E11.5 to E18.5, the mutant mice manifested very low levels of these proteins during the same developmental stages (Fig. 4C,D). On the other hand, Tim23 retained an unchanged expression pattern during the same period (Fig. 4C,D).

Development (2021) 148, dev199026. doi:10.1242/dev.199026

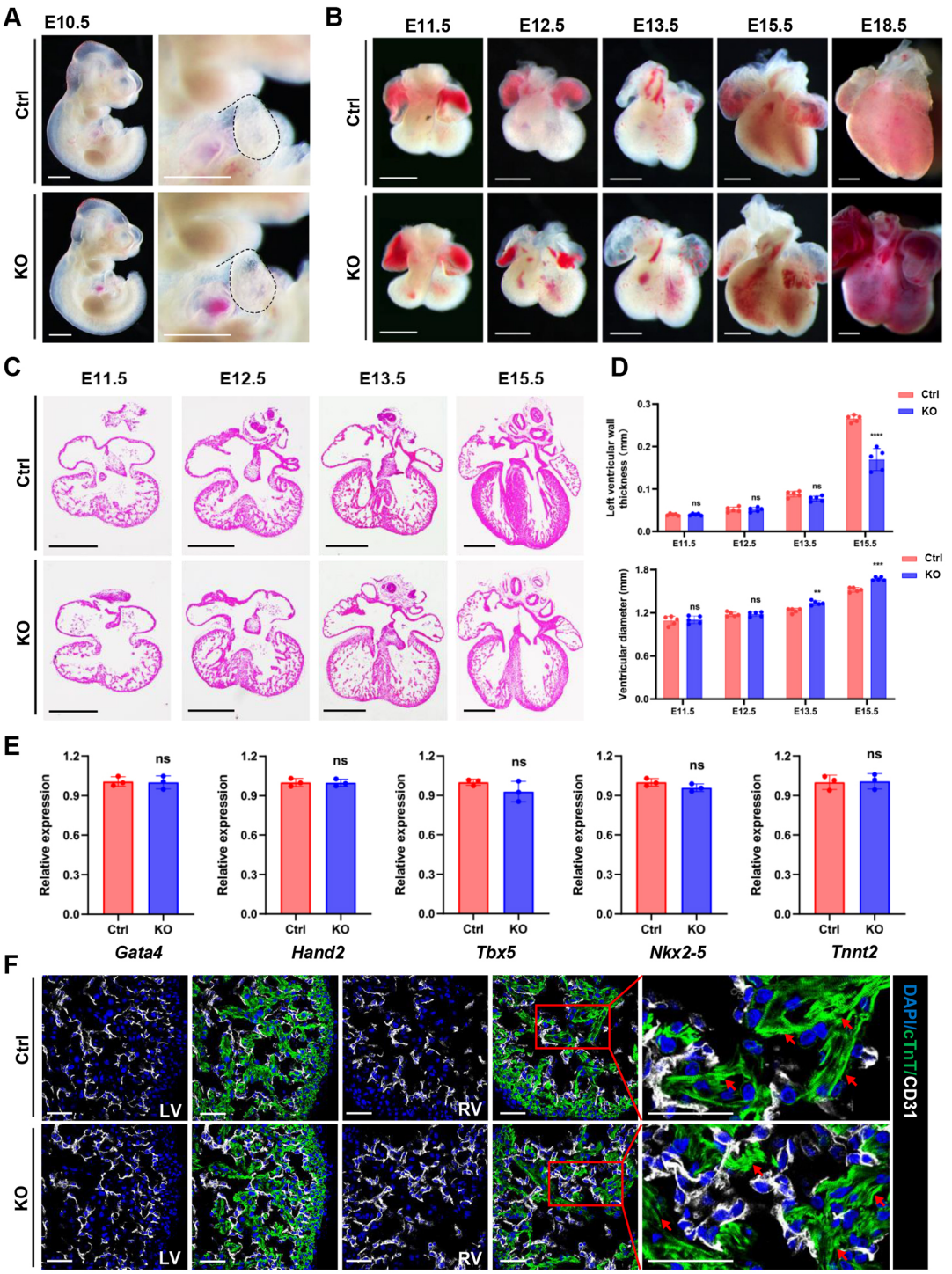

Fig. 3. The SRCAP complex played a pivotal role during the mid-to-late period of heart development. (A,B) Gross analysis of embryos and hearts. Knockout (KO; bottom) was *Tnnt2-Cre*-mediated deletion. (A) Embryos at E10.5. The right panels depicted the outflow tract together with the right ventricle (dashed lines). The mice in the two groups were comparable. (B) Heart of *Znhit1* deletion mice showed anomalies from E12.5 and manifested the feature of heart failure at E18.5. (C,D) Histological analysis (C) and quantification (D) of left ventricular wall thickness and ventricular diameter. (E) Quantitative analysis of mRNA expression level in E11.5 heart. (F) Immunofluorescence staining of E12.5 heart. Red arrows in far right panels (showing magnification of boxed areas) indicate the sarcomere. *Znhit1* deletion did not affect the structure of endocardium and sarcomere. LV, left ventricle; RV, right ventricle. Data are mean±s.e.m. ***P*<0.01, ****P*<0.001, *****P*<0.0001 (two-tailed unpaired Student's *t*-test or two-way ANOVA). ns, not significant. Scale bars: 500 µm (A,B,C); 50 µm (F).

We further examined the mRNA level of the genes encoding these respiratory chain subunits and did not find a reduction in the *Znhit1* mutant (Fig. S6). These results suggest that, although SRCAP remodeler did not regulate these respiratory chain subunits at a transcriptional level, it was necessary to sustain the protein stability of these subunits. Lastly, measurement of the amount of ATP revealed a remarkable reduction in the mutant heart (Fig. 4E).

Overall, these studies revealed a crucial role of the SRCAP complex in maintaining the integrity of mitochondrial morphology and the respiratory complex.

Development (2021) 148, dev199026. doi:10.1242/dev.199026

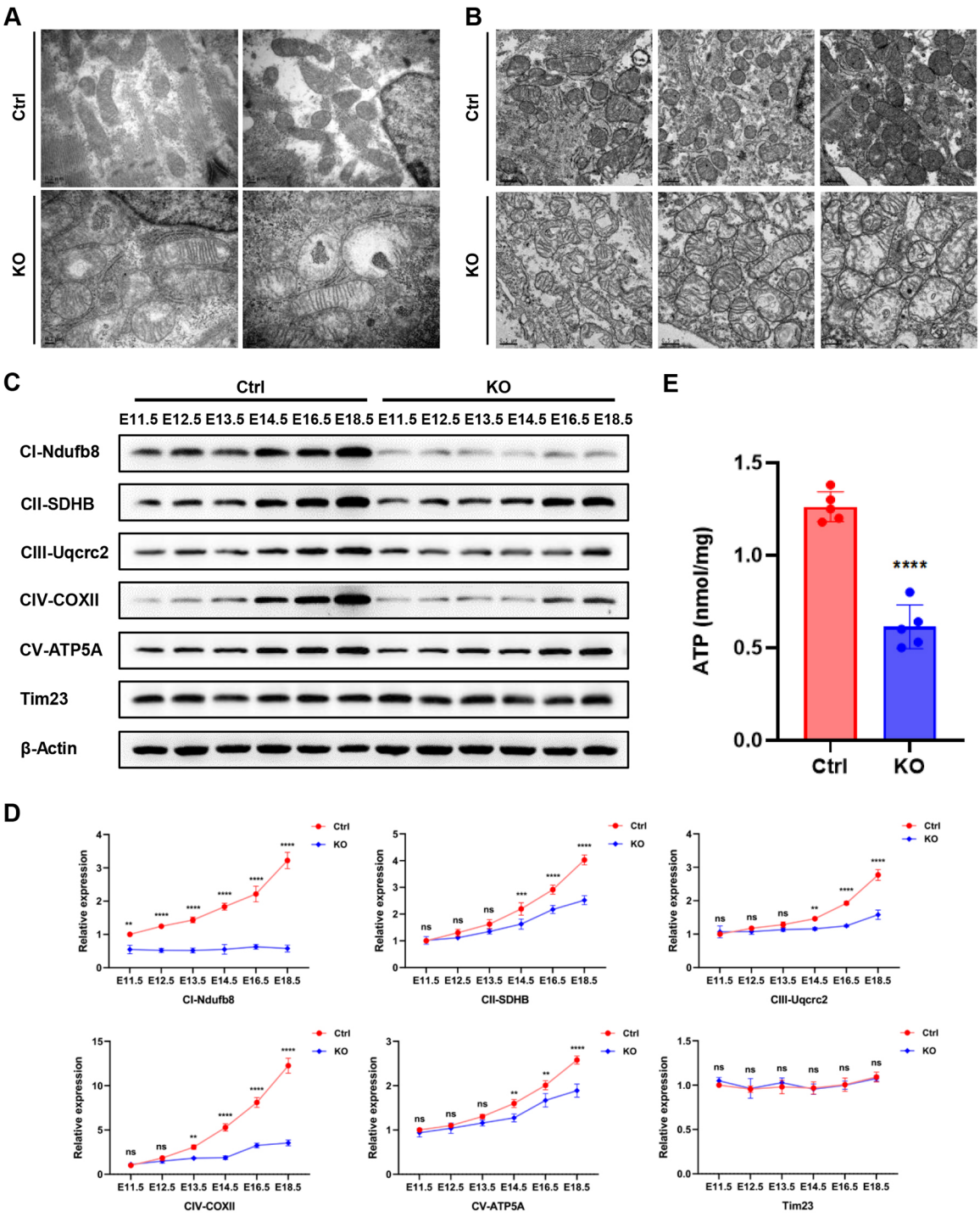

Fig. 4. The SRCAP complex maintained the integrity of mitochondrial morphology and respiratory complexes. (A) Transmission electron microscope (TEM) images display the mitochondria in the cardiomyocytes of left ventricles at E14.5. Knockout (KO; bottom) was *Tnnt2-Cre*-mediated *Znhit1* deletion. The mitochondrial cristae were destroyed in the KO mice. (B) TEM images display the mitochondria in the cardiomyocytes of right ventricles at E13.5. KO was *Mef2c-AHF-Cre*-mediated *Znhit1* deletion. Mitochondria in the KO mice were swollen with damaged cristae. (C,D) Western blot analysis (C) and quantification (D). β-Actin served as loading control. (E) Measurement of ATP in the heart tissue at E14.5. Data are mean±s.e.m. ***P*<0.01, ****P*<0.001, *****P*<0.0001 (two-tailed unpaired Student's *t*-test or two-way ANOVA). ns, not significant. Scale bars: 0.2 µm (A); 0.5 µm (B).

Central function of the SRCAP complex in regulating mitochondrial oxidative metabolism

Next, we performed transcriptome analysis to compare gene expression difference between control and *Znhit1* mutants. For this, heart tissues from both *Tnnt2-Cre*-mediated *Znhit1*-deletion and *Mef2c-AHF-Cre*-mediated *Znhit1*-deletion mice, together with those from control mice, were collected for RNA-seq analysis. The heatmap displays downregulation of a majority of genes in the mutant mice compared with control, indicating that the SRCAP complex primarily activated gene transcription (Fig. 5A-D). Gene Ontology (GO) enrichment analysis of the downregulated genes uncovered mitochondrion- and metabolic-related biological

Development (2021) 148, dev199026. doi:10.1242/dev.199026

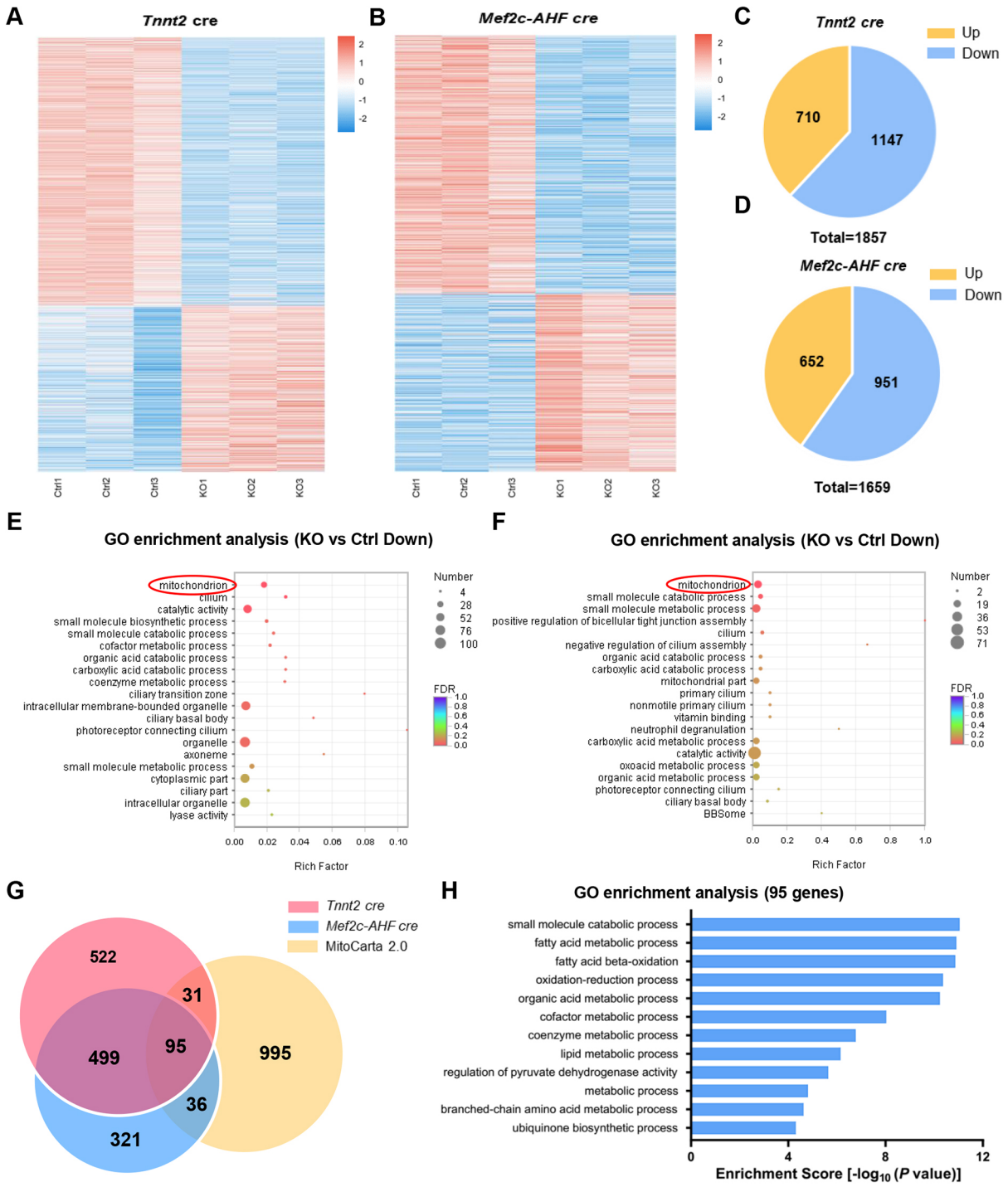

Fig. 5. Identification of the SRCAP-regulatory biological pathways and target genes. (A-D) Heatmap (A,B), and up- and downregulated genes (C,D) in *Znhit1* deletion mice (heart tissues at E12.5). The SRCAP complex primarily activated gene expression. (E,F) GO enrichment analysis of downregulated genes in *Znhit1* deletion mice (*Tnnt2 Cre*, E; *Mef2c-AHF Cre*, F). Mitochondrial-related genes were most conspicuously enriched. (G) Venn diagram depicting the overlapping of the downregulated genes in *Tnnt2-Cre*-mediated (red) and *Mef2c-AHF-Cre*-mediated (blue) *Znhit1* deletion mice together with the mitochondrial genes in MitoCarta 2.0 database (yellow). (H) GO enrichment analysis of the 95 overlapped genes in G.

processes (Fig. 5E,F). A comparison of those mitochondrial function-related genes that were downregulated in both groups together with the database of MitoCarta 2.0 identified 95 overlapping genes (Fig. 5G). GO enrichment analysis of the 95 genes revealed that all of them participated in metabolic processes (Fig. 5H). Among them were crucial components of fatty acid β-oxidation, ETC, TCA and related processes, and the branched-chain amino acid (BCAA) metabolic process (Table 2). We also analyzed 363 upregulated genes in both *Tnnt2 Cre*- and *Mef2c-AHF-Cre*-mediated *Znhit1* deletion mice (Fig. S7A). The results showed enrichment for p53 signaling as well as genes negatively regulating cell proliferation, which was consistent with our observation that proliferation was significantly decreased in *Znhit1*-deletion hearts (Fig. S7B). The cAMP signaling pathway

Development (2021) 148, dev199026. doi:10.1242/dev.199026

Table 2. Identification of mitochondrial metabolic genes downregulated in Znhit1 mutant heart

Metabolic pathway and genes	Functions
Fatty acid metabolic process	
Cpt2	Transports long-chain fatty acids to mitochondria
Echs1	Functions in the fatty acid β-oxidation pathway
Ech1	Functions in the auxiliary step of the fatty acid β-oxidation pathway
Gcdh	Catalyzes oxidative decarboxylation of glutaryl-CoA
Acad11	Functions in the fatty acid beta-oxidation pathway
Acsf3	Functions in malonate metabolism
Phyh	Functions in the oxidation of branched fatty acids
Mecr	Functions in mitochondrial fatty acid synthesis
Oxsm	Functions in mitochondrial fatty acid synthesis
Electron transport chain	
Coq3	Functions in coenzyme Q biosynthesis
Coq4	Functions in coenzyme Q biosynthesis
Coq7	Functions in coenzyme Q biosynthesis
Ndufaf6	Respiratory chain member
Citrate cycle (TCA) and TCA-related processes	
Ogdhl	Participates in the formation of succinyl CoA
Pcx	Participates in the formation of oxaloacetate
Pdp2	Activates the pyruvate dehydrogenase complex
D2hgdh	Participates in the formation of α-ketoglutarate
Pcca	Participates in the formation of succinyl CoA
Branched-chain amino acid (BCAA) metabolic process	
Ivd	Catalyzes the third step in leucine catabolism
Bckdha	Catalyzes the irreversible reactions in BCAA catabolism
Bckdhb	Catalyzes the irreversible reactions in BCAA catabolism

TCA, tricarboxylic acid cycle

and genes related to cardiac contraction and extracellular matrix assembly were also highly enriched (Fig. S7B). Collectively, these results unveiled the central function of the SCRAP complex in regulating mitochondrial oxidative metabolism.

Chromatin profiling determination of the SRCAP-accessible regions in the metabolic genes

CUT&Tag chromatin profiling was conducted using an antibody against H2A.Z and heart tissues to map the SRCAP remodeler accessible regions in the genome (Kaya-Okur et al., 2019). It was found that approximately half of the regions accessed by the SRCAP complex were promoter areas (Fig. 6A). Although chromosomal landscape manifested a dense profile in the control mice, it became sparse in the mutant (Fig. 6B). We found that ∼76% of the promoter-associated H2A.Z peaks were decreased in the mutant knockout (KO) compared with control. In particular, 39 genes were affected among the 95 candidate mitochondrial genes, suggesting that the expression of these 39 genes might be directly regulated by the SRCAP complex. A detailed analysis and comparison revealed a sharp reduction of peaks in the promoter regions of crucial metabolic genes including *Coq3*, *Coq4*, *Ogdhl*, *Cpt2* and *Echs1* in mutant mice compared with controls (Fig. 6C). Among them, *Coq3* and *Coq4* are required for CoQ10 biosynthesis, *Ogdhl* (oxoglutarate dehydrogenase like) encodes a protein similar to alpha-ketoglutarate dehydrogenase, a rate-limiting enzyme for the TCA cycle, *Cpt2* (carnitine palmitoyl transferase-2) encodes an obligatory enzyme for long chain fatty acid oxidation and the protein product of the *Echs1* gene (enoyl-CoA hydratase, short chain 1) functions in the second step of the mitochondrial fatty acid β-oxidation pathway. All of these genes are essential for aerobic metabolism and cellular respiration. Quantitative PCR and western blotting analysis confirmed the profoundly reduced expression level of these genes and proteins in mutant hearts compared with controls (Fig. 6D-F). In addition, 12 genes out of the 13 required for biosynthesis of CoQ10 showed markedly reduced expression level in *Znhit1* mutant mice (Fig. S8). In conclusion, the SRCAP remodeler directly regulates the expression of a panel of essential genes in the aerobic metabolic pathways including fatty acid β-oxidation, TCA cycle, ETC activity and oxidative phosphorylation (OXPHOS).

DISCUSSION

This study brings to light the physiological function of the SRCAP remodeler in regulating mitochondrial maturation and metabolic shift during heart development. This remodeler functions as a master regulator of mitochondrial metabolism through modulating gene expression involved in fatty acid β-oxidation, TCA cycle, biosynthesis of CoQ10 and protein stability of respiratory chain complexes (Fig. 7).

In contrast to the SWI/SNF complex, the SRCAP complex does not regulate cardiac progenitor specification and cardiomyocyte differentiation, which take place before E10.5. Instead, this complex specifically monitors multiple metabolic events and processes in the mitochondria from E10.5 and safeguards the continuously increased metabolic activity to meet the demands from heart development and contraction. The temporal window of E10.5-E14.5 was a crucial turning point for mitochondrial morphogenesis and maturation, and metabolic switch from anaerobic glycolysis to oxidative metabolism (fatty acid oxidation, TCA, ETC activity and OXPHOS).

Our results suggest that the SRCAP complex is important to maintain the stability of respiratory chain complexes. Disturbance of the SRCAP complex failed to affect the gene transcription of the core components, but their protein level substantially declined. It has been previously reported that mitochondrial cristae remodeling and damage would disrupt the respiratory super-complexes (Cogliati et al., 2013), and we therefore speculate that the reduced protein levels of the respiratory chain subunits might be a consequence of defective mitochondrial cristae. On the other hand, cardiolipin is the signature phospholipid of mitochondria and is abundantly enriched in the inner mitochondrial membrane for maintenance of the respiratory super-complexes (Paradies et al., 2014). Cardiolipin is synthesized by cardiolipin synthase (encoded by *Crls1*). We performed a detailed study of *Crls1* in our CUT&Tag assay data, and found that *Crls1* expression could be directly regulated by the SRCAP complex. Disruption of the SRCAP complex significantly reduced *Crls1* expression level (Fig. S9A,B). Thus, it is plausible to propose that reduction of *Crls1* expression might impair the stability of the respiratory complexes as a second effect to *Znhit1* loss of function. Therefore, the SRCAP complex governs mitochondrial maturation and metabolism at two tiers: transcriptionally, this complex controls the expression of genes involved in fatty acid β-oxidation, TCA cycle and CoQ10 biosynthesis (OXPHOS); at protein level, the SRCAP complex maintains the stability of respiratory chain complexes (Fig. 7).

Although VHL-HIF signaling regulates anaerobic glycolysis before E12.5, the SRCAP complex promotes oxidative metabolism from ∼E12.5 to birth. The coordination of these two regulatory machineries guarantees the completion of the metabolic switch during embryonic heart development.

This study sheds light on understanding the transcriptional regulation of CoQ10 biosynthesis that requires at least 13 genes. Disruption of the SRCAP complex abolished the expression of 12

Development (2021) 148, dev199026. doi:10.1242/dev.199026

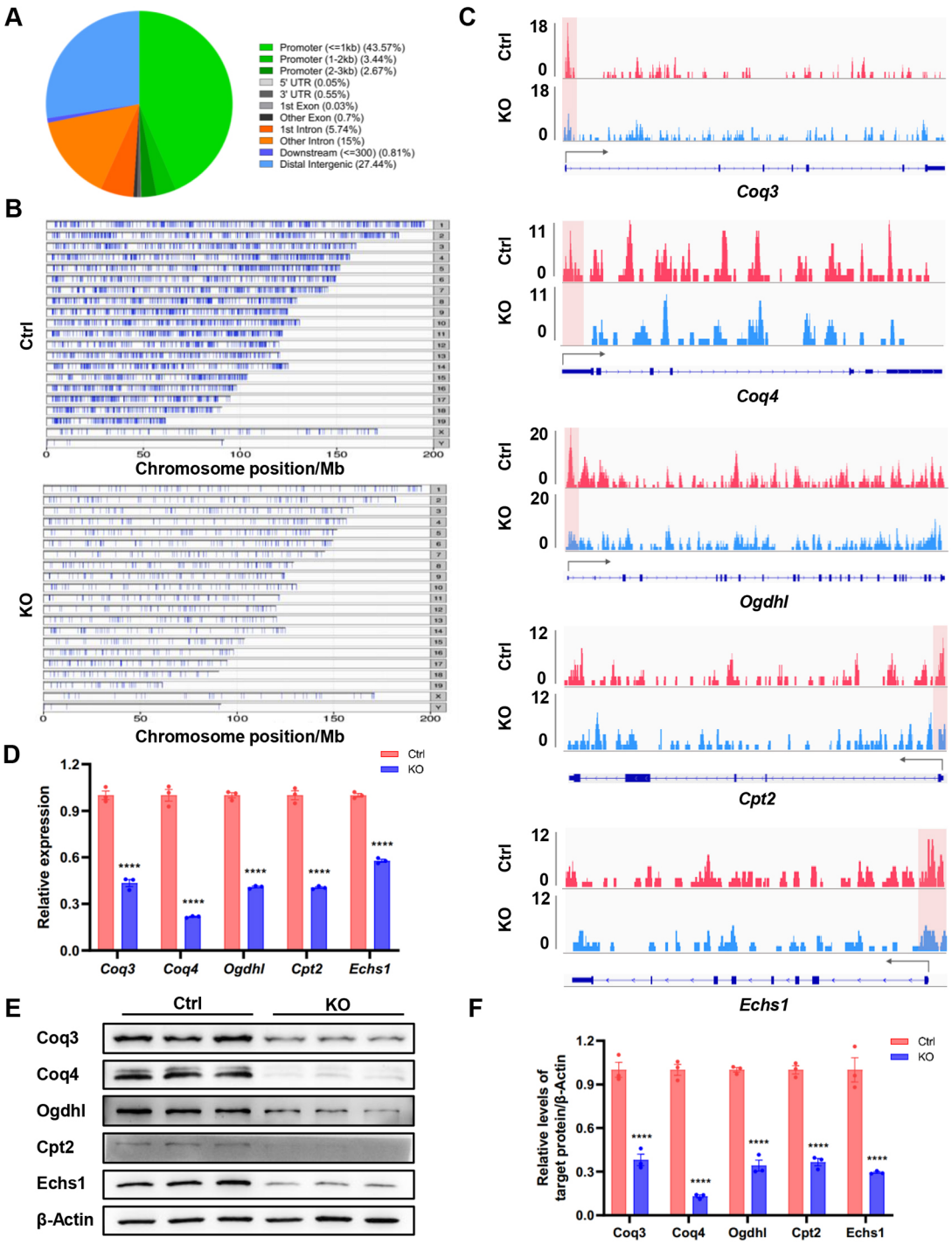

Fig. 6. Chromatin profiling determination of the SRCAP accessible regions in the metabolic genes. (A-C) CUT&Tag assay of H2A.Z-enriched regions in the heart at E13.5. H2A.Z is mainly deposited in the promoter region of genes (A). Chromosomal landscape (B) shows loss of *Znhit1* significantly reduces the deposition of H2A.Z. (C) Genome browser view of the distribution of the reads of *Coq3*, *Coq4*, *Ogdhl*, *Cpt2* and *Echs1*. The deposition of H2A.Z in the promoter region of these genes was significantly reduced. (D) qRT-PCR examination of gene expression at E13.5. (E,F) Western blot analysis (E) and quantification (F) of heart tissues from E13.5 mice. Data are mean±s.e.m. ****P<0.0001 (two-way ANOVA).

out of these 13 genes. Thus, the SRCAP complex is the first identified regulator of CoQ10 biosynthesis.

In human, defects in the enzymes or transport proteins in the metabolic pathways can cause serious metabolic disorders, leading to neurological disease, heart defects and cardiomyopathy. Among them, an increasing number of patients afflicted by primary deficiency with CoQ10, OGDHL, CPT2 and ECHS1 have been diagnosed. Our study helps decipher the pathogenesis of these ailments and may provide therapeutic applications to treat these diseases.

MATERIALS AND METHODS

Mice

The previously described mouse strains used in this study included *Znhit1*-floxed (Zhao et al., 2019), *Tnnt2-Cre* (Wu et al., 2010), *Mef2c-AHF-Cre*

Development (2021) 148, dev199026. doi:10.1242/dev.199026

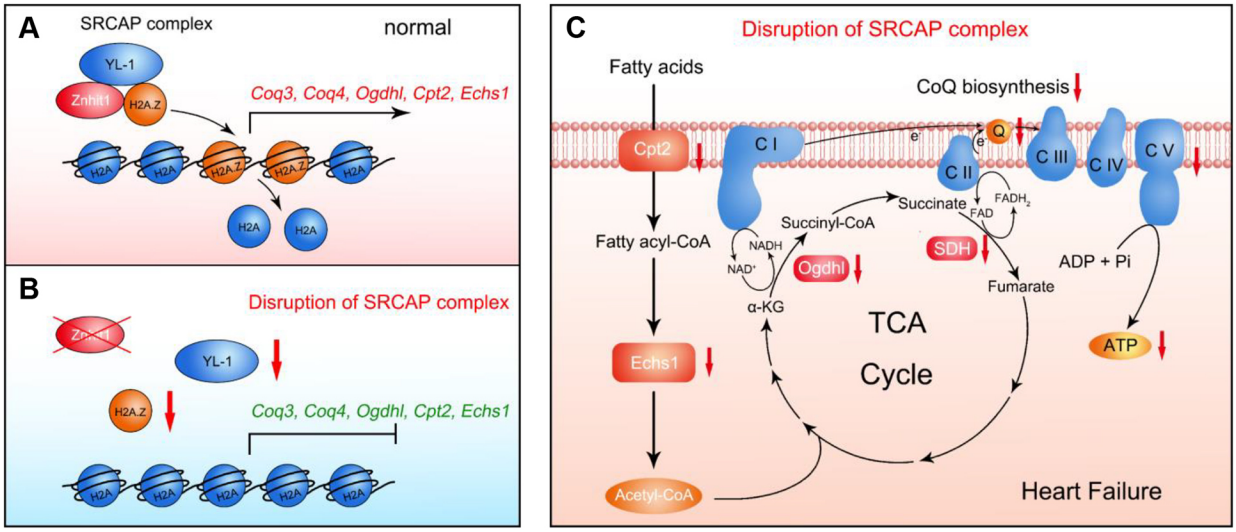

Fig. 7. Working models. (A) Under normal condition, Znhit1 associates with YL-1 and H2A.Z to participate in the SRCAP chromatin remodeling complex, which modulates the replacement of H2A with H2A. Z in the nucleosomes to activate expression of genes involved in oxidative metabolism. (B) Removal of *Znhit1* leads to the disruption of the SRCAP complex resulting in suppression of target gene expression. (C) Aberrant SRCAP remodeler causes transcriptional defects of a panel of essential genes involved in the aerobic metabolic pathways including fatty acid β-oxidation, tricarboxylic acid cycle, electron transport chain activity and oxidative phosphorylation. Meanwhile, the stability of respiratory chain complexes is disrupted. As a result, cardiomyocyte oxidative metabolism is greatly impaired, leading to developmental anomalies and heart failure.

(Xia et al., 2019) and *ERT2-Cre* (from The Jackson Laboratory, Stock No: 008463) mice. All mouse lines were maintained on the C57BL/6 background. Mice were group-housed in accordance with the regulations on mouse welfare and ethics of Nanjing University, with 12 h/12 h light-dark cycles and had *ad libitum* access to food and water. The Institutional Animal Care and Use Committee (IACUC) of the Model Animal Research Center of Nanjing University approved all animal procedures used in this study.

Western blot

Tissues and cells were washed with cold PBS and lysed on ice with RIPA buffer [50 mM Tris-HCl (pH 7.4), 150 mM NaCl, 1% TritonX-100, 0.1% SDS, 1% Na-deoxycholate, 1 mM EDTA] containing protease inhibitor cocktail (Roche) and PhosSTOP (Roche) for 30 min. Supernatant fractions were collected after centrifugation at 12,000 rpm (13,500 ***g***) for 10 min at 4°C, and protein concentration was quantified by BCA Protein Assay Kit (Beyotime, P0012). After separation via SDS-PAGE, proteins were transferred to PVDF membranes (Millipore), blocked in 5% non-fat milk or bovine serum albumin and incubated with appropriate primary antibodies (Table S1). Membranes were cut and sections probed separately to reduce wastage of samples.

Quantitative real-time PCR

Total RNA from cells or heart ventricles was isolated using TRIzol reagent (Invitrogen), and reversely translated into cDNA using HiScript III 1st Strand cDNA Synthesis Kit (Vazyme, R312-01). Real-Time PCR was performed in MicroAmp™ Optical 96-Well Reaction Plate with Barcode & Optical Caps (Applied Biosystems) using Hieff UNICON® qPCR SYBR Green Master Mix (Yeasen). Reactions were carried out on the QuantStudio™ 5 Real-Time PCR System (Applied Biosystems). All primers used in qRT-PCR are listed in Table S2. Triplicate amplifications were carried out for each target gene and the housekeeping genes *Gapdh*, *Actb* and relative expression values were calculated using the ΔΔCt analysis method.

Immunofluorescence (IF) staining

For paraffin sections, hearts were fixed overnight in 4% paraformaldehyde (PFA) at 4°C, rinsed several times in PBS, dehydrated in an ethanol series, then paraffin embedded and sectioned at 7 µm using a Leica RM2016 microtome. During the staining process, the paraffin sections were dewaxed, rehydrated and submerged in preheated sodium citrate solution (pH 6.0) for antigen retrieval. The slides were then cooled down and blocked in goat serum for 1 h at room temperature, washed with PBS and incubated in primary antibodies diluted in blocking solution overnight at 4°C. The following day, slides were washed three times in PBS and incubated with secondary antibodies for 2 h at room temperature, washed three times in PBS and mounted in 50% glycerol before confocal imaging.

For cryosections, hearts were fixed in 4% PFA for 1 h on ice, washed in PBS and incubated in 30% sucrose solution overnight at 4°C. The following day, hearts were embedded in OCT medium, and then snap frozen in liquid nitrogen and stored at −80°C. Then, 7 µm-thick cryosections were obtained using a Leica CM1950 automated Cryostat. For IF staining, sections were thawed at room temperature for 15 min, washed in PBS, blocked in goat serum and incubated in primary antibodies overnight at 4°C. Next, the slides were washed in PBS, and incubated in secondary antibodies for 2 h at room temperature followed by washes in PBS and mounted in 50% glycerol before confocal imaging. Details of all antibodies used are in Table S1.

Isolation and culture of MEFs

Znhit1$^{f/f}$ and *Znhit1*$^{f/f}$*; ERT2-Cre* MEFs were derived from E13.5 embryos. After removal of the head and intestinal organs, each embryo was washed with ice-cold PBS. Embryo bodies were minced and digested with 1 mL trypsin solution (0.25% Trypsin-EDTA, 25200056, Gibco™) for 15 min at 37°C and 5% CO_2. Then Trypsin-EDTA incubation was stopped with 8 mL complete media [high-glucose DMEM (12800017, Gibco™) supplemented with 10% fetal bovine serum (FSP500, Excell Bio) and 100 U/ml Penicillin-Streptomycin (15140122, Gibco™)], vigorously pipetted several times and incubated at 37°C and 5% CO_2. Expression of Cre recombinase was induced by treating with 0.5 mM 4-OH-Tamoxifen (H7904, Sigma-Aldrich) for 3 days, and then cells were harvested for western blot analysis. We used MEFs within three passages in our experiments to avoid replicative senescence.

RNAi

For RNAi analysis of Znhit1 in HeLa cells, a 21-nucleotide small interfering RNA (siRNA) duplex was synthesized as follows: sense, 5′-GCCUCAG-UUUGAUGACGAUTT-3′; antisense, 5′-AUCGUCAUCAAACUGAGG-CTT-3′. siRNA with sense 5′-UUCUCCGAACGUGUCACGUTT-3′ and

antisense 5′-ACGUGACACGUUCGGAGAATT-3′ was used as negative control. For RNAi analysis of Znhit1 in H9C2 cells, a 21-nucleotide siRNA duplex was synthesized as follows: sense 5′-CCGACAGUUGGAGGCAUUATT-3′ and antisense 5′-UAAUGCCUCCAACUGUCGGTT-3′. siRNA with sense 5′-UUCUCCGAACGUGUCACGUTT-3′ and antisense 5′-ACGUGACACGUUCGGAGAATT-3′ was used as negative control. Transfections were performed using Lipo3000 (Invitrogen) and GP-Transfect mate (GenePharma) according to the manufacturers' instructions. Cells were harvested for western blot analysis.

RNA-seq

RNA quality was determined using the 2100 Bioanalyser (Agilent) and quantified using the ND-2000 (NanoDrop Technologies). Only a high-quality RNA sample (OD260/280=1.8~2.2, OD260/230≥2.0, RIN≥6.5, 28S:18S≥1.0, >2 µg) was used to construct the sequencing library. The RNA-seq transcriptome library was prepared using the TruSeq™ RNA sample preparation Kit from Illumina using 1 µg of total RNA and sequenced with the Illumina HiSeq xten/NovaSeq 6000 sequencer (2×150 bp read length). The raw paired end reads were trimmed and quality controlled by SeqPrep and Sickle with default parameters. Then clean reads were separately aligned to reference genome with orientation mode using TopHat (Trapnell et al., 2009) software. The mapping criteria of bowtie was as follows: sequencing reads should be uniquely matched to the genome allowing up to two mismatches, without insertions or deletions. The expression level of each transcript was calculated according to the fragments per kilobase of exon per million mapped reads (FRKM) method. R statistical package software EdgeR (Robinson et al., 2010) was used for differential expression analysis.

CUT&Tag assay

Cardiomyocytes isolated from E13.5 mouse heart ventricle were used for the CUT&Tag assay. Chromatin immunoprecipitation was performed as previously described (Tao et al., 2020) using H2A.Z antibody (ab4174, Abcam, 1:50) and Hyperactive *In-Situ* ChIP Library Prep Kit for Illumina (pG-Tn5) (TD901-02, Vazyme) according to the manufacturer's protocol. CUT&Tag libraries were generated using TruePrep® Index Kit V2 for Illumina (TD202, Vazyme) according to the manufacturer's protocol. Final CUT&Tag libraries were sequenced with the Illumina Nova6000 sequencer. Reads were quality trimmed by Fastp (0.19.11) and mapped to mouse genome (mm10) by BWA (0.7.12-r1039). MACS2 was used with default parameters (Zhang et al., 2008) to call peaks. Genome-wide core motifs were found for H2A.Z using HOMER [scanMotifGenomeWide.pl (v4.9.1)]. Scatterplots, correlation plots and heatmaps are displayed using deepTools (v 3.0.2).

Statistical analysis

Statistical analyses and graphics were produced with GraphPad Prism 8.0 software. Datasets were compared by two-tailed unpaired Student's *t*-test or two-way ANOVA with *P*-values adjusted for multiple tests. A value of $P<0.05$ (*) was considered statistically significant, whereas $P<0.01$(**), $P<0.001$(***) and $P<0.0001$(****) were considered statistically very significant. All results are presented as mean±s.e.m.

Acknowledgements

We thank Dr Bin Zhou from Albert Einstein College of Medicine for providing the *Tnnt2-Cre* mice.

Competing interests

The authors declare no competing or financial interests.

Author contributions

Conceptualization: M.X., W.Z., Z.Y.; Methodology: M.X., W.Z.; Formal analysis: Z.Y.; Investigation: M.X., J.Y., Y.S., H.Y.; Resources: X.L., Z.Y.; Writing - original draft: Z.Y.; Writing - review & editing: Z.Y.; Supervision: Z.Y.; Project administration: Z.Y.

Funding

This work was supported by grants from the National Key Research and Development Program of China (2019YFA0801601) and from the National Natural Science Foundation of China (31930029 and 91854111) to Z.Y.

Data availability

RNA-seq and CUT&Tag data have been deposited in the SRA database under accession numbers PRJNA702882, PRJNA702867 and PRJNA699727.

Peer review history

The peer review history is available online at https://journals.biologists.com/dev/article-lookup/148/8/dev199026/

References

Beckwith, S. L., Schwartz, E. K., Garcia-Nieto, P. E., King, D. A., Gowans, G. J., Wong, K. M., Eckley, T. L., Paraschuk, A. P., Peltan, E. L., Lee, L. R. et al. (2018). The INO80 chromatin remodeler sustains metabolic stability by promoting TOR signaling and regulating histone acetylation. *PLoS Genet.* **14**, e1007216. doi:10.1371/journal.pgen.1007216

Bruneau, B. G. and Srivastava, D. (2014). Congenital heart disease: entering a new era of human genetics. *Circ. Res.* **114**, 598-599. doi:10.1161/CIRCRESAHA.113.303060

Cheong, A., Archambault, D., Degani, R., Iverson, E., Tremblay, K. D. and Mager, J. (2020). Nuclear-encoded mitochondrial ribosomal proteins are required to initiate gastrulation. *Development* **147**, dev188714. doi:10.1242/dev.188714

Clapier, C. R. and Cairns, B. R. (2009). The biology of chromatin remodeling complexes. *Annu. Rev. Biochem.* **78**, 273-304. doi:10.1146/annurev.biochem.77.062706.153223

Cogliati, S., Frezza, C., Soriano, M. E., Varanita, T., Quintana-Cabrera, R., Corrado, M., Cipolat, S., Costa, V., Casarin, A., Gomes, L. C. et al. (2013). Mitochondrial Cristae shape determines respiratory chain supercomplexes assembly and respiratory efficiency. *Cell* **155**, 160-171. doi:10.1016/j.cell.2013.08.032

Cuadrado, A., Corrado, N., Perdiguero, E., Lafarga, V., Munoz-Canoves, P. and Nebreda, A. R. (2010). Essential role of p18(Hamlet)/SRCAP-mediated histone H2A.Z chromatin incorporation in muscle differentiation. *EMBO J.* **29**, 2014-2025. doi:10.1038/emboj.2010.85

Cui, M., Wang, Z., Bassel-Duby, R. and Olson, E. N. (2018). Genetic and epigenetic regulation of cardiomyocytes in development, regeneration and disease. *Development* **145**, dev171983. doi:10.1242/dev.171983

Doimo, M., Desbats, M. A., Cerqua, C., Cassina, M., Trevisson, E. and Salviati, L. (2014). Genetics of Coenzyme Q10 Deficiency. *Molecular Syndromology* **5**, 156-162. doi:10.1159/000362826

Dong, S. L., Han, J. H., Chen, H. X., Liu, T., Huen, M. S. Y., Yang, Y. R., Guo, C. X. and Huang, J. (2014). The Human SRCAP Chromatin Remodeling Complex Promotes DNA-End Resection. *Curr. Biol.* **24**, 2097-2110. doi:10.1016/j.cub.2014.07.081

Guimaraes-Camboa, N., Stowe, J., Aneas, I., Sakabe, N., Cattaneo, P., Henderson, L., Kilberg, M. S., Johnson, R. S., Chen, J., McCulloch, A. D. et al. (2015). HIF1 alpha Represses cell stress pathways to allow proliferation of hypoxic fetal cardiomyocytes. *Dev. Cell* **33**, 507-521. doi:10.1016/j.devcel.2015.04.021

Hardie, D. G. (2014). AMPK-Sensing energy while talking to other signaling pathways. *Cell Metab.* **20**, 939-952. doi:10.1016/j.cmet.2014.09.013

Hom, J. R., Quintanilla, R. A., Hoffman, D. L., de Mesy Bentley, K. L., Molkentin, J. D., Sheu, S. S. and Porter, G. A. Jr. (2011). The permeability transition pore controls cardiac mitochondrial maturation and myocyte differentiation. *Dev. Cell* **21**, 469-478. doi:10.1016/j.devcel.2011.08.008

Hota, S. K. and Bruneau, B. G. (2016). ATP-dependent chromatin remodeling during mammalian development. *Development* **143**, 2882-2897. doi:10.1242/dev.128892

Kathiriya, I. S., Nora, E. P. and Bruneau, B. G. (2015). Investigating the transcriptional control of cardiovascular development. *Circ. Res.* **116**, 700-714. doi:10.1161/CIRCRESAHA.116.302832

Kaya-Okur, H. S., Wu, S. J., Codomo, C. A., Pledger, E. S., Bryson, T. D., Henikoff, J. G., Ahmad, K. and Henikoff, S. (2019). CUT&Tag for efficient epigenomic profiling of small samples and single cells. *Nat. Commun.* **10**, 1930. doi:10.1038/s41467-019-09982-5

Larsson, N.-G., Wang, J., Wilhelmsson, H., Oldfors, A., Rustin, P., Lewandoski, M., Barsh, G. S. and Clayton, D. A. (1998). Mitochondrial transcription factor A is necessary for mtDNA maintance and embryogenesis in mice. *Nat. Genet.* **18**, 231-236. doi:10.1038/ng0398-231

Maroli, G. and Braun, T. (2020). The long and winding road of cardiomyocyte maturation. *Cardiovasc. Res.* **117**, 712-726. doi:10.1093/cvr/cvaa159

Menendez-Montes, I., Escobar, B., Palacios, B., Gomez, M. J., Izquierdo-Garcia, J. L., Flores, L., Jimenez-Borreguero, L. J., Aragones, J., Ruiz-Cabello, J., Torres, M. et al. (2016). Myocardial VHL-HIF signaling controls an embryonic metabolic switch essential for cardiac maturation. *Dev. Cell* **39**, 724-739. doi:10.1016/j.devcel.2016.11.012

Meng, Z. X., Li, S., Wang, L., Ko, H. J., Lee, Y., Jung, D. Y., Okutsu, M., Yan, Z., Kim, J. K. and Lin, J. D. (2013). Baf60c drives glycolytic metabolism in the muscle and improves systemic glucose homeostasis through Deptor-mediated Akt activation. *Nat. Med.* **19**, 640-645. doi:10.1038/nm.3144

Morrison, A. J. (2020). Chromatin-remodeling links metabolic signaling to gene expression. *Mol. Metab.* **38**, 100973. doi:10.1016/j.molmet.2020.100973
Paradies, G., Paradies, V., Ruggiero, F. M. and Petrosillo, G. (2014). Cardiolipin and mitochondrial function in health and disease. *Antioxid Redox Sign* **20**, 1925-1953. doi:10.1089/ars.2013.5280
Robinson, M. D., McCarthy, D. J. and Smyth, G. K. (2010). edgeR: a Bioconductor package for differential expression analysis of digital gene expression data. *Bioinformatics* **26**, 139-140. doi:10.1093/bioinformatics/btp616
Sardiu, M. E., Gilmore, J. M., Groppe, B. D., Herman, D., Ramisetty, S. R., Cai, Y., Jin, J. J., Conaway, R. C., Conaway, J. W., Florens, L. et al. (2015). Conserved abundance and topological features in chromatin-remodeling protein interaction networks. *EMBO Rep.* **16**, 116-126. doi:10.15252/embr.201439403
Tao, X., Feng, S., Zhao, T. and Guan, X. (2020). Efficient chromatin profiling of H3K4me3 modification in cotton using CUT&Tag. *Plant Methods* **16**, 120. doi:10.1186/s13007-020-00664-8
Trapnell, C., Pachter, L. and Salzberg, S. L. (2009). TopHat: discovering splice junctions with RNA-Seq. *Bioinformatics* **25**, 1105-1111. doi:10.1093/bioinformatics/btp120
Waardenberg, A. J., Ramialison, M., Bouveret, R. and Harvey, R. P. (2014). Genetic networks governing heart development. *Cold Spring Harb. Perspect Med.* **4**, a013839. doi:10.1101/cshperspect.a013839
Wang, Y. and Hekimi, S. (2016). Understanding Ubiquinone. *Trends Cell Biol.* **26**, 367-378. doi:10.1016/j.tcb.2015.12.007
Watanabe, S., Radman-Livaja, M., Rando, O. J. and Peterson, C. L. (2013). A histone acetylation switch regulates H2A.Z deposition by the SWR-C remodeling enzyme. *Science* **340**, 195-199. doi:10.1126/science.1229758
Wong, M. M., Cox, L. K. and Chrivia, J. C. (2007). The chromatin remodeling protein, SRCAP, is critical for deposition of the histone variant H2A.Z at promoters. *J. Biol. Chem.* **282**, 26132-26139. doi:10.1074/jbc.M703418200
Wu, B., Zhou, B., Wang, Y., Cheng, H. L., Hang, C. T., Pu, W. T., Chang, C. P. and Zhou, B. (2010). Inducible cardiomyocyte-specific gene disruption directed by the rat Tnnt2 promoter in the mouse. *Genesis* **48**, 63-72. doi:10.1002/dvg.20573
Xia, M., Luo, W., Jin, H. and Yang, Z. (2019). HAND2-mediated epithelial maintenance and integrity in cardiac outflow tract morphogenesis. *Development* **146**, dev177477. doi:10.1242/dev.177477
Ye, B. Q., Liu, B. Y., Yang, L. L., Huang, G. L., Hao, L., Xia, P. Y., Wang, S., Du, Y., Qin, X. W., Zhu, P. P. et al. (2017). Suppression of SRCAP chromatin remodelling complex and restriction of lymphoid lineage commitment by Pcid2. *Nat. Commun.* **8**, 1518. doi:10.1038/s41467-017-01788-7
Zhang, Y., Liu, T., Meyer, C. A., Eeckhoute, J., Johnson, D. S., Bernstein, B. E., Nusbaum, C., Myers, R. M., Brown, M., Li, W. et al. (2008). Model-based analysis of ChIP-Seq (MACS). *Genome Biol.* **9**, R137. doi:10.1186/gb-2008-9-9-r137
Zhao, B., Chen, Y., Jiang, N., Yang, L., Sun, S., Zhang, Y., Wen, Z., Ray, L., Liu, H., Hou, G. et al. (2019). Znhit1 controls intestinal stem cell maintenance by regulating H2A.Z incorporation. *Nat. Commun.* **10**, 1071. doi:10.1038/s41467-019-09060-w

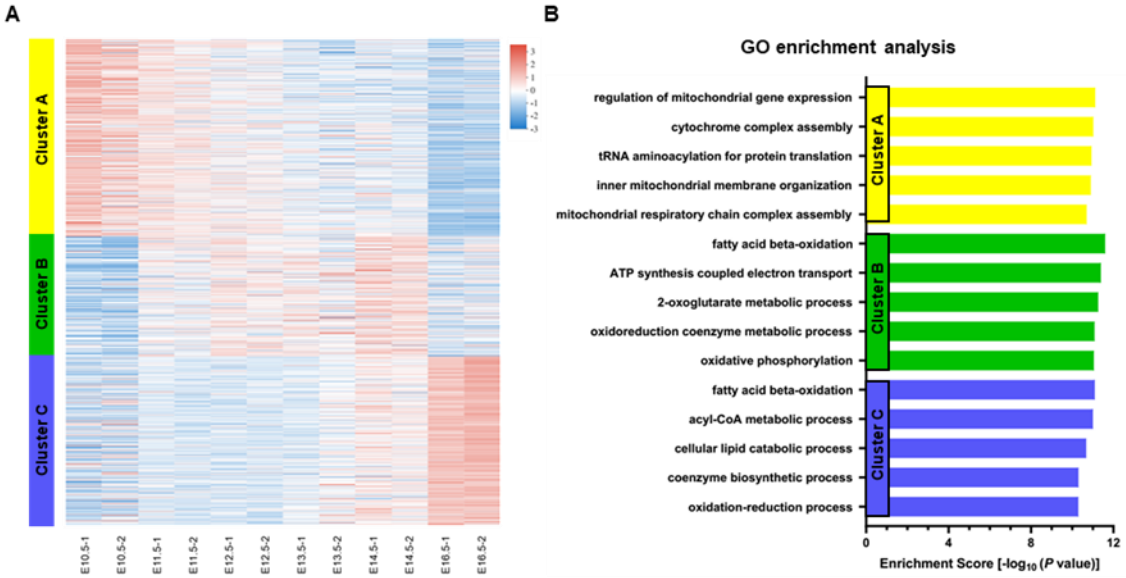

Fig. S1. Analysis of mitochondrial genes during heart development. (A) Heatmap. Three clusters of genes with distinct temporal expression patterns were categorized. **(B)** GO enrichment analysis.

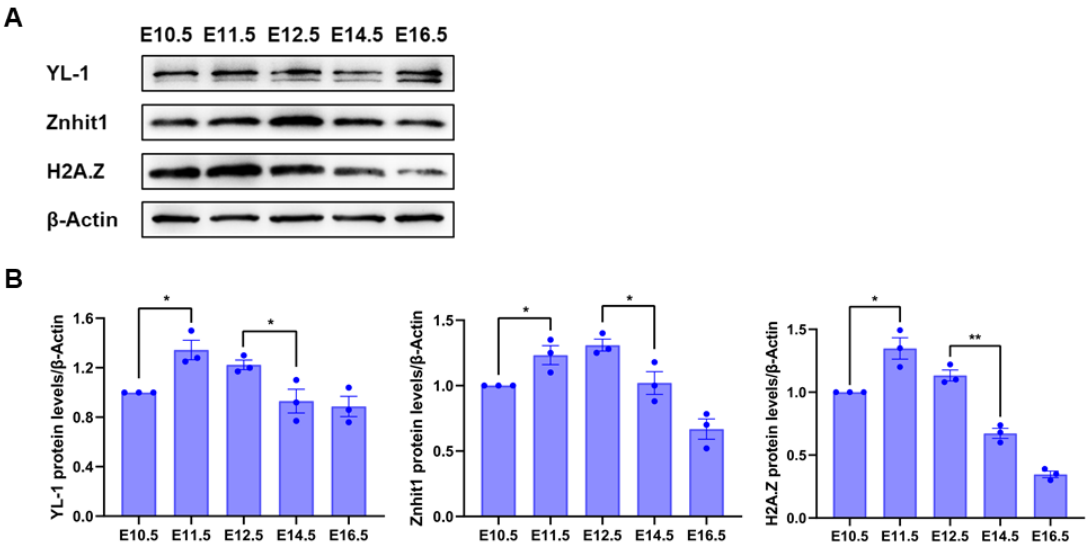

Fig. S2. The temporal expression pattern of the core subunits of SRCAP complex. **(A)** Western blotting analysis. **(B)** Quantification of **(A)**. Experiments were repeated independently for three times, which produced similar results. Data are mean ± s.e.m. Student's t test: **P* < 0.05, ***P* < 0.01.

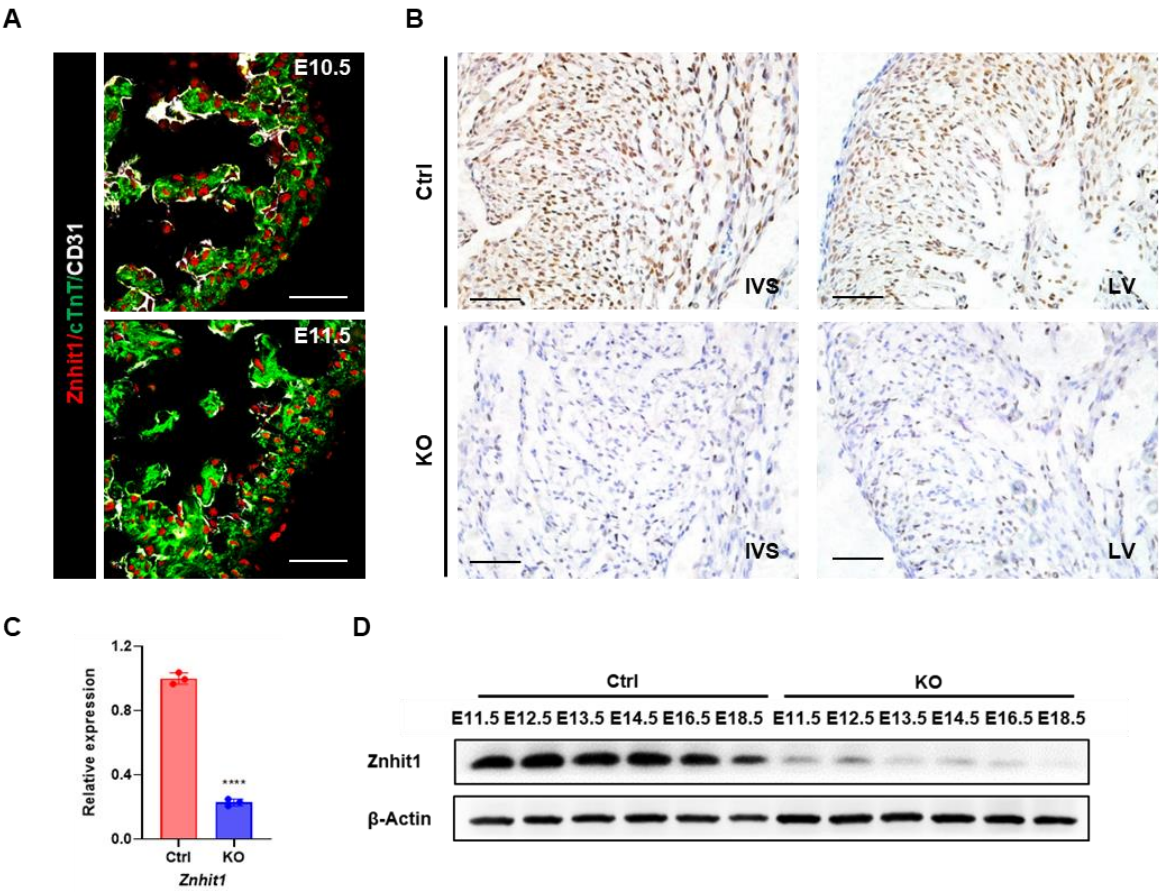

Fig. S3. Verification of *Znhit1* deletion in the heart tissues. (A) Immuno-fluoresence staining. Znhit1 was localized in the nuclei of cardiomyocytes at both E10.5 and E11.5. **(B-D)** Specific knock out *Znhit1* in cardiomyocytes by *Tnnt2*-Cre. **(B)** Immunohistochemical analysis of Znhit1 in the heart. IVS, interventricular septum; LV, left ventricle. Scale bar=50μm. **(C)** qRT-PCR analysis of *Znhit1* expression in the heart at E11.5 with normalization to *Gapdh* levels. Data are mean ± s.e.m. Student's t test: ****$P < 0.0001$. **(D)** Western blot analysis of Znhit1. β-Actin serves as loading control. Ctrl was control heart and KO was *Znhit1* deletion heart (*Tnnt2*-Cre mediated deletion).

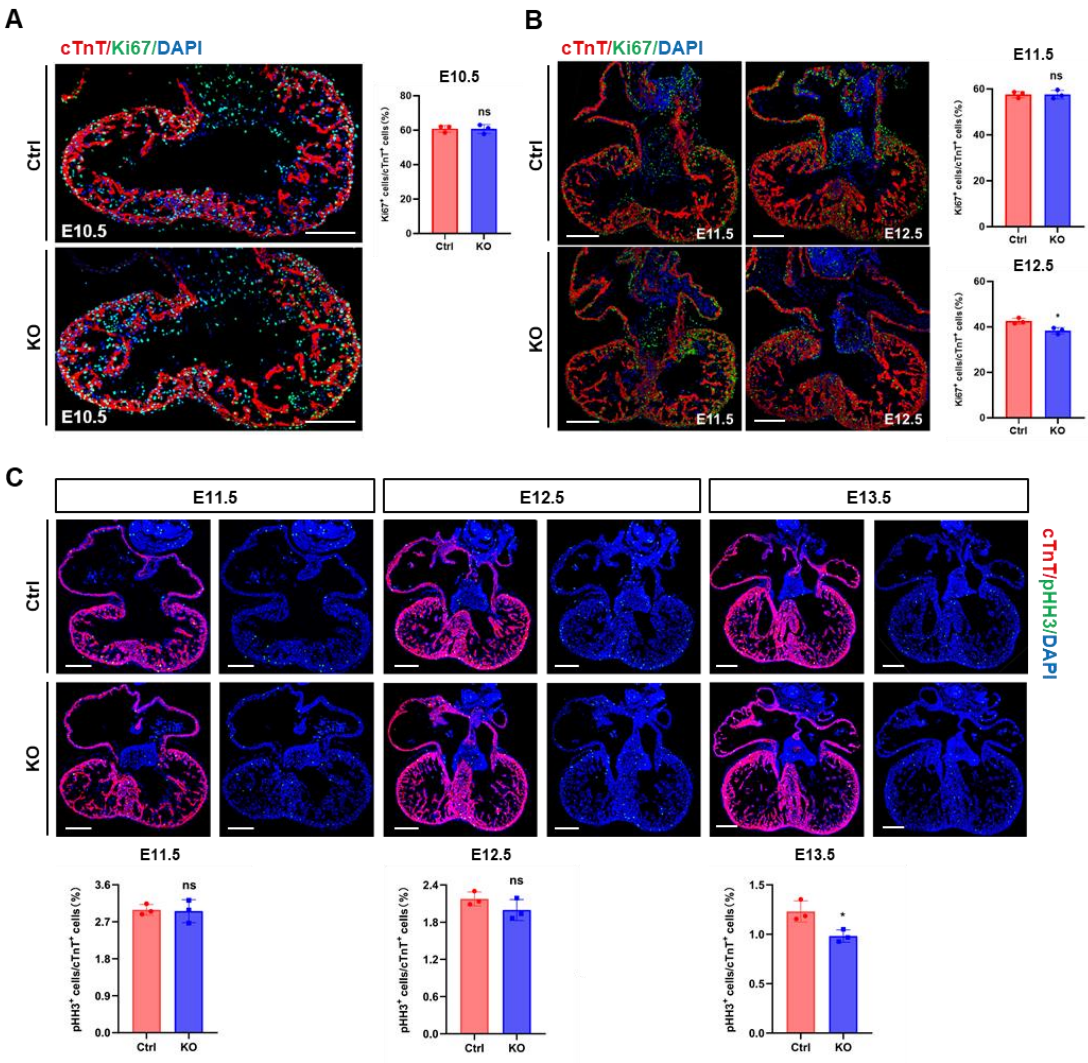

Fig. S4. Decreased cell proliferation of cardiomyocytes in the heart of *Znhit1* deletion mice. Ctrl was control heart and KO was *Znhit1* deletion heart (*Tnnt2*-Cre mediated deletion). **(A** and **B)** Ki67 immunostaining and quantification of proliferating cardiomyocytes ($Ki67^{+}cTnT^{+}$ cells). **(C)** pHH3 immuno-staining and quantification of proliferating cardiomyocytes ($pHH3^{+}cTnT^{+}$ cells). Data are mean ± s.e.m. Student's t test: $*P < 0.05$. ns, not significant. Scale bar= 200μm.

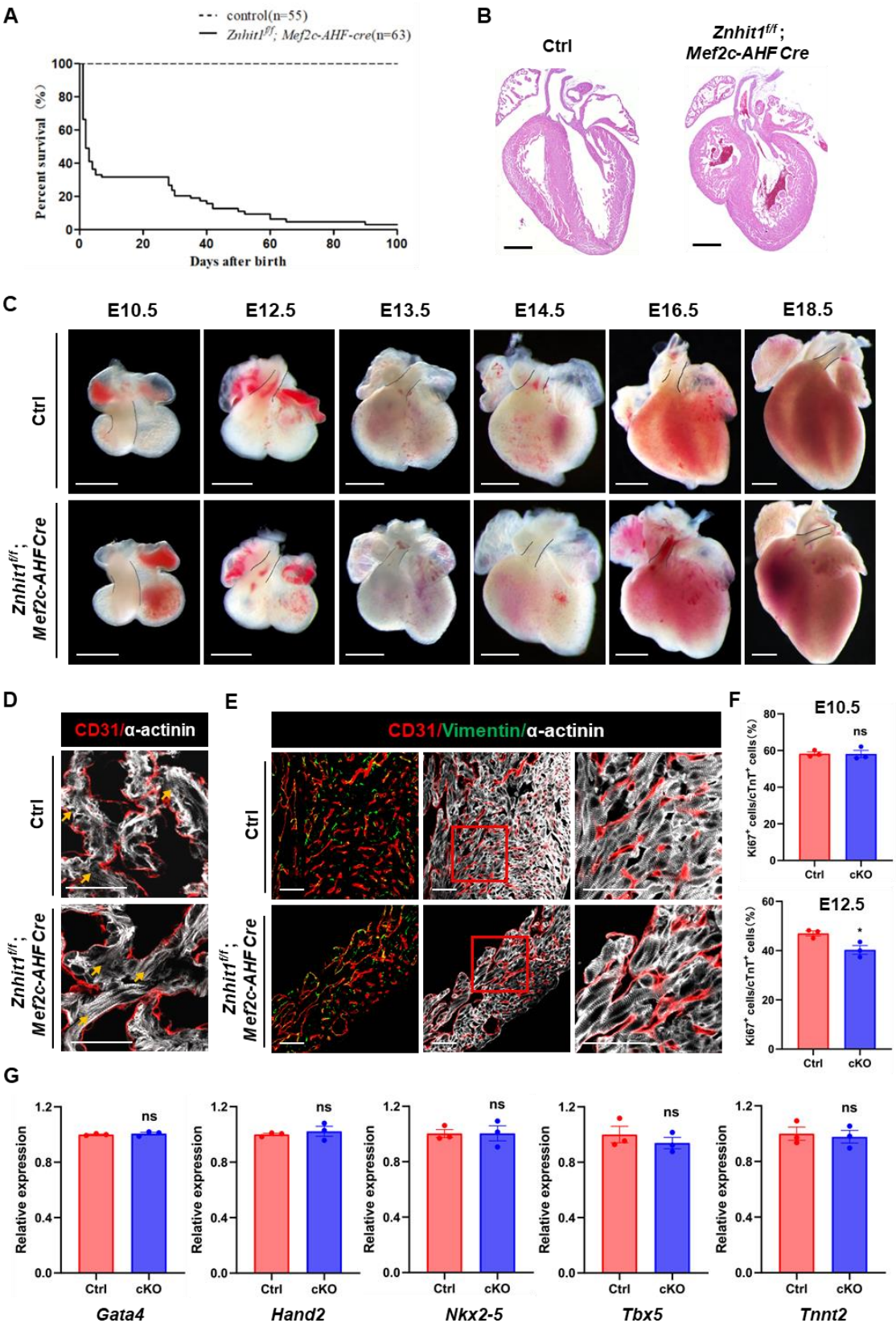

Fig. S5. Disruption of the SRCAP complex did not affect the early development of AHF-progenitor cells. (A) Survival curves. **(B)** H&E staining of P1 heart sections. Scale bars: 500μm. **(C)** Gross analysis of the hearts. Black lines depicted the outflow tract or pulmonary artery (PA). Slight PA stenosis was observed in the KO heart from

E13.5. Scale bars: 500μm. **(D** and **E)** Fluorescence staining of the right ventricle at E12.5 **(D)** and E18.5 **(E)** α-actinin (in white) labeled sarcomere, and CD31 (in red) indicated endocardium and coronary endothelial cells. Yellow arrows pointed to the sarcomere in **(D)**. **(E)** The rightmost panels were higher magnification of the boxer area in the adjacent left panels. Scale bars: 50μm. No big difference was found between the mice of the two groups. **(F)** Quantification of proliferating cardiomyocytes. **(G)** Quantitative analysis of mRNA expression level in the right ventricle at E11.5. Data are mean ± s.e.m. Student's t test: $*P < 0.05$. ns, not significant.

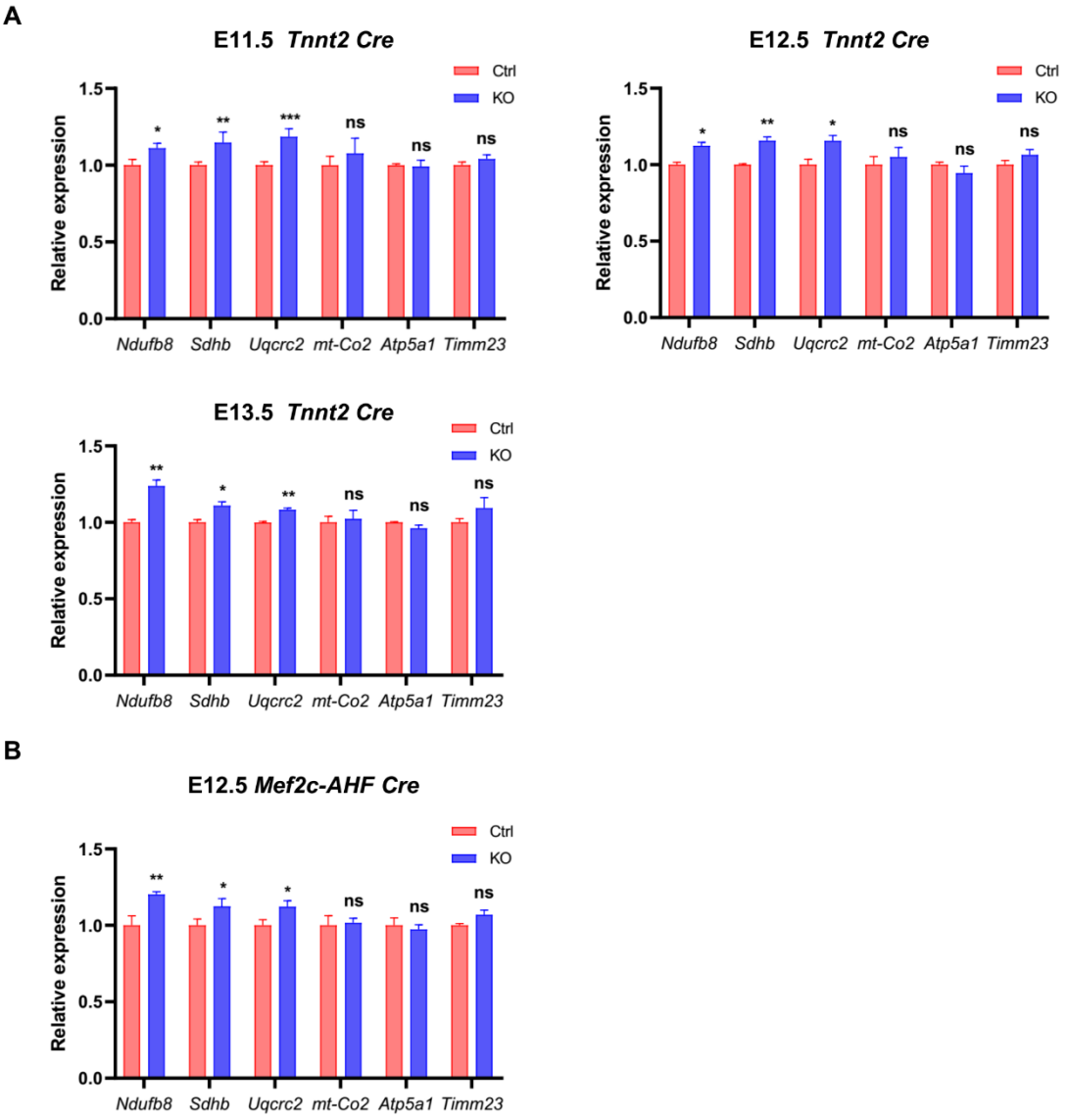

Fig. S6. Analysis of mRNA levels by qRT-PCR in the heart tissues. (A) qRT-PCR analysis of E11.5, E12.5 and E13.5 hearts. **(B)** qRT-PCR analysis of E12.5 right ventricles. Data are mean ± s.e.m. Two-way ANOVA: *$P < 0.05$, **$P < 0.01$, ***$P < 0.001$. ns, not significant.

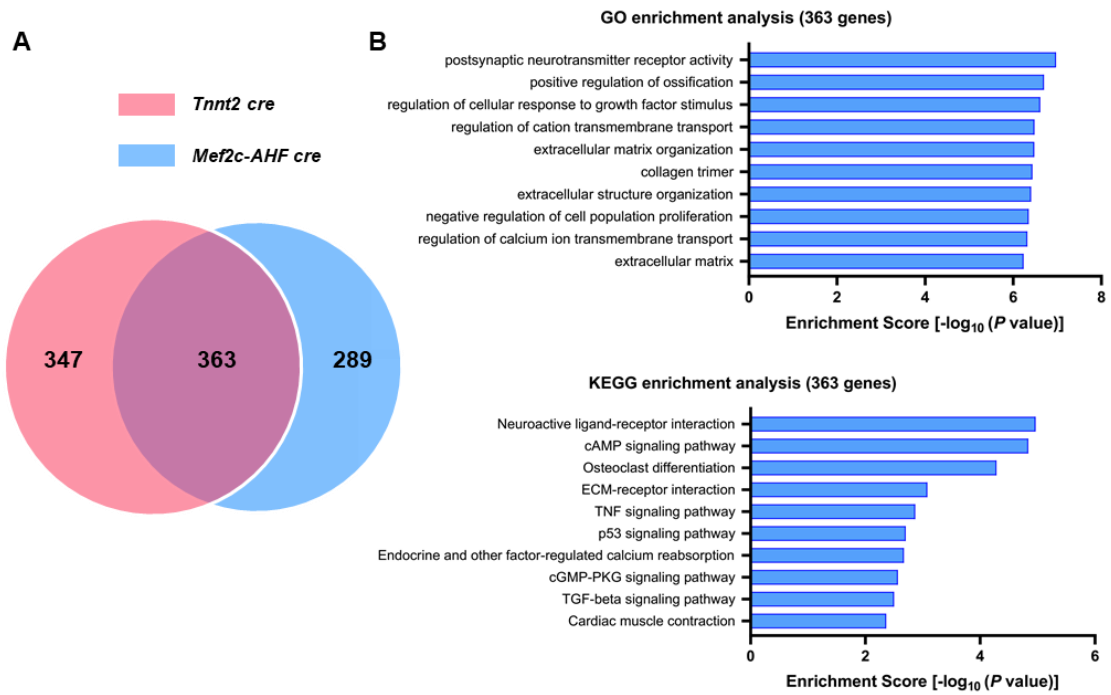

Fig. S7. Analysis of the up-regulated genes in the *Znhit1* mutant mice. (A) Venn diagram depicting the overlapping of the up-regulated genes in *Tnnt2* Cre (in red) and *Mef2c-AHF* Cre (in blue) mediated *Znhit1* deletion mice. **(B)** GO and KEGG enrichment analysis of the 363 overlapping genes in **(A)**.

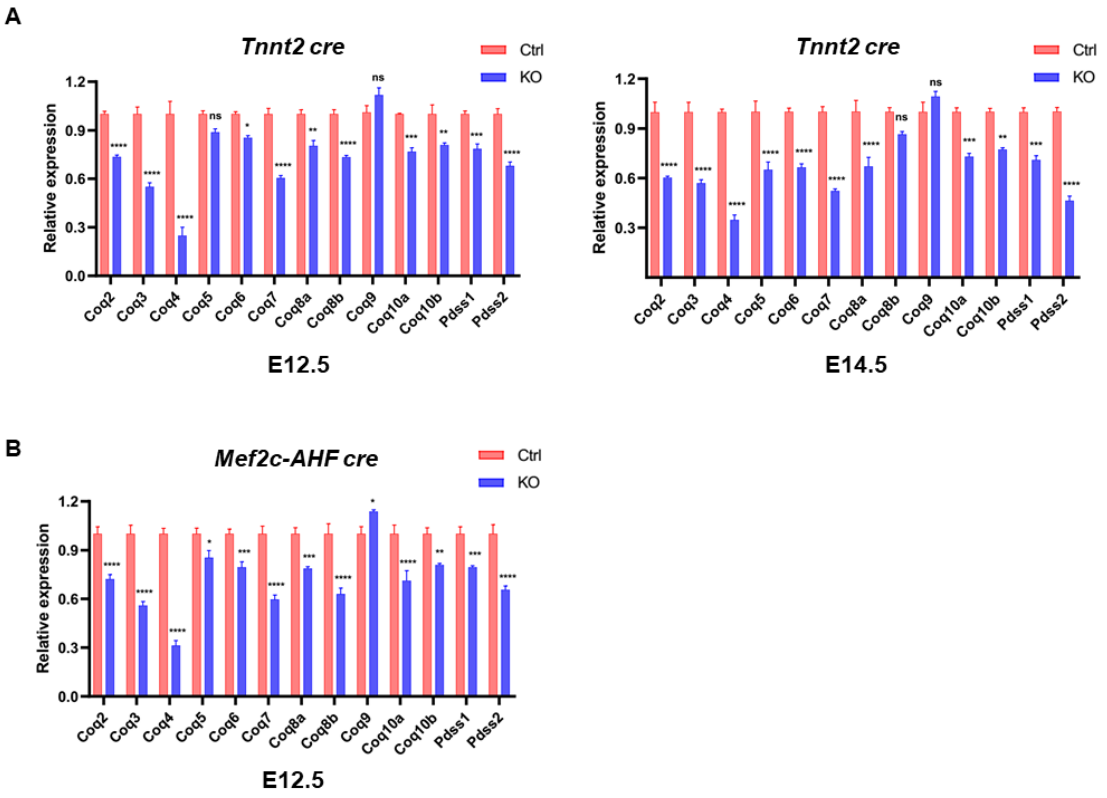

Fig. S8. 12 genes out of the 13 genes required for biosynthesis of CoQ showed markedly reduced expression level in *Znhit1* mutant mice. (A) qRT-PCR analysis of E12.5 and E14.5 hearts. **(B)** qRT-PCR analysis of E12.5 right ventricles. Data are mean ± s.e.m. Two-way ANOVA: *$P < 0.05$, **$P < 0.01$, ***$P < 0.001$, ****$P < 0.0001$. ns, not significant.

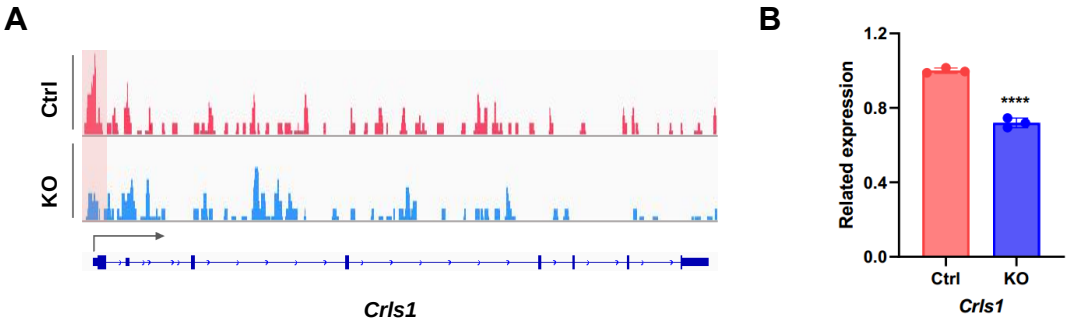

Fig. S9. *Crls1* was a direct regulatory target of the SRCAP complex. (A) CUT & Tag assay of H2A.Z-enriched regions in the heart at E13.5. The peak at the promoter region of *Crls1* was reduced in the KO. (B) qRT-PCR examination of *Crls1* expression level at E13.5. Data are mean ± s.e.m. Student's t test: ****$P < 0.0001$.

Table S1. Primary antibodies

Antibodies	Applications	Dilution	Species	Source	Catalog number
Ndufb8	WB	1:1000	Rabblt	Proteintech	14794-1-AP
SDHB	WB	1:1000	Rabblt	abcam	ab178423
Uqcrc2	WB	1:1000	Rabblt	Proteintech	14742-1-AP
COXII	WB	1:2000	Rabblt	Proteintech	55070-1-AP
COXIV	WB	1:10000	Rabblt	Proteintech	11242-1-AP
Atp5A	WB	1:1000	Rabblt	Proteintech	14676-1-AP
Tim23	WB	1:2000	Mouse	BD	611223
AMPKα	WB	1:1000	Rabblt	CST	#2532
Phospho-AMPKα (Thr172)	WB	1:1000	Rabblt	CST	#2535
β-Actin	WB	1:10000	Mouse	Bioworld	BS6007M
YL-1	WB	1:1000	Rabblt	Proteintech	15143-1-AP
Histone H2A.Z	WB	1:1000	Rabblt	abcam	ab4174
Histone H2A.Z	WB	1:1000	Rabblt	abcam	ab150402
Znhit1	WB	1:1000	Rabblt	abcam	ab238125
ZNHIT1	WB	1:1000	Rabblt	Proteintech	16595-1-AP
Coq3	WB	1:1000	Rabblt	Proteintech	28051-1-AP
Coq4	WB	1:1000	Rabblt	Proteintech	16654-1-AP
Ogdhl	WB	1:1000	Rabblt	Proteintech	17110-1-AP
Echs1	WB	1:1000	Rabblt	Proteintech	11305-1-AP
Cpt2	WB	1:1000	Rabblt	Proteintech	26555-1-AP
Cardiac Troponin T	IF	1:500	Mouse	Life	MA5-12960
Vimentin	IF	1:200	Rabbit	Santa Cruz	sc-5565
CD31	IF	1:200	Rat	BD	550274
a-Actinin	IF	1:200	Mouse	Sigma	A7811
Ki67	IF	1:2000	Rabbit	abcam	ab15580
Phospho-Histone H3	IF	1:200	Rabbit	CST	#9701

Table S2. Primers for qRT-PCR.

Genes	Primer sequence (5' to 3')	Genes	Primer sequence (5' to 3')
Znhit1	F: CAGACGGCGAGACAAGTTC R: CAAACTGAGGTAGCCTCTTGC	*Cpt2*	F: CAGCACAGCATCGTACCCA R: TCCCAATGCCGTTCTCAAAAT
Gata4	F: CCCTACCCAGCCTACATGG R: ACATATCGAGATTGGGGTGTCT	*Echs1*	F: TTGTGAACTTGCCATGATGTGT R: TGCTCGGGTGAGTCTCTGAG
Hand2	F: GAGAACCCCTACTTCCACGG R: GACAGGGCCATACTGTAGTCG	*Ogdhl*	F: AGCGGAGTCAGCTCCAGTTAT R: GGATCTGGTAGGCCCGGAT
Tbx5	F: ATGGCCGATACAGATGAGGG R: TTCGTGGAACTTCAGCCACAG	*Coq2*	F: ACAAGCCCATAGGAACCTGG R: CTCCACGCATCAGAATAGCTC
Nkx2-5	F: GACAAAGCCGAGACGGATGG R: CTGTCGCTTGCACTTGTAGC	*Coq3*	F: CTCGTGGGGTTCGTCTCCT R: GAGCTGCGTCCCTGAGTAAG
Tnnt2	F: TCTTCTGGTGCTACTCGAAGC R: CTCCATCGGGGATCTTGGGT	*Coq4*	F: TGTACCCGGACCACATCCC R: AACCATGTCGTGGCGATAGG
Mef2c	F: ATCCCGATGCAGACGATTCAG R: AACAGCACACAATCTTTGCCT	*Coq5*	F: CCCAGGTGCTGCGTTCTATG R: GTCTCAAACCCGAAGTGCG
Acta2	F: GTCCCAGACATCAGGGAGTAA R: TCGGATACTTCAGCGTCAGGA	*Coq6*	F: CTCAGCAGTTTTGGTGCATGG R: TGTCCCTGTCGAACATTATCAAG
Ndufb8	F: TGTTGCCGGGGTCATATCCTA R: AGCATCGGGTAGTCGCCATA	*Coq7*	F: CTCATCATCAGGTGTCACAGTTC R: GGTTTGCTCCATATTCACCAGC
Sdhb	F: AATTTGCCATTTACCGATGGGA R: AGCATCCAACACCATAGGTCC	*Coq8a*	F: GCAGAGCGCATTGTGAGTACA R: GCCAGGTGAGGGTTGATGAAG
Uqcrc2	F: AAAGTTGCCCCGAAGGTTAAA R: GAGCATAGTTTTCCAGAGAAGCA	*Coq8b*	F: GAGAGGATCGTGCAGACCTTA R: TAAAGTCGGCACTCTGTCGGA
mt-Co2	F: AACCATAGGGCACCAATGATAC R: GGATGGCATCAGTTTTAAGTCC	*Coq9*	F: GTGGGGTTCCGGTCTTCAG R: GGGGTGGACGGGAAAACTC
Atp5a1	F: TCTCCATGCCTCTAACACTCG R: CCAGGTCAACAGACGTGTCAG	*Coq10a*	F: CCAACGTCCAGGAGTACCG R: GGTGGAAACCCAACCTCCAAT
Timm23	F: GAAGGTGGCGGAAGAAGTAGC R: GGGGGTTCATACCAGTCAGC	*Coq10b*	F: GGAGACTATTTGGCGTTTTAGCC R: AAGAACAGAGTAGCGAGCTGA
Gapdh	F: AACTTTGGCATTGTGGAAGG R: ACACATTGGGGGTAGGAACA	*Pdss1*	F: ACACCAGCAATGTGCAGTTG R: ACAGACCTTTCAAGTCTCTCCAG
Actb	F: GGCTGTATTCCCCTCCATCG R: CCAGTTGGTAACAATGCCATGT	*Pdss2*	F: CGCTTGTCCGGTTACCTCG R: GGGTAGCCCACGATCTTCTC